J. Fluid Mech. (2003), *vol.* 489, *pp.* 199–228.
DOI: 10.1017/S0022112003004993 Printed in the United Kingdom

Non-circular baroclinic beta-plane modons: constructing stationary solutions

By Z. KIZNER[1,2], D. BERSON[1] AND R. KHVOLES[2]

[1]Department of Physics, Bar-Ilan University, Ramat-Gan 52900, Israel

[2]Department of Mathematics, Bar-Ilan University, Ramat-Gan 52900, Israel

(Received 17 July 2002 and in revised form 20 January 2003)

Conditions determining the existence of localized steadily translating two-layer vortices (modons) of arbitrary symmetric form on the β-plane are considered. A numerical method for direct construction of modon solutions is suggested and its accuracy is analysed in relation to the parameters of the computational procedure and the geometrical and physical parameters of the modon sought. Using this method, several non-circular baroclinic solutions are constructed marked by nonlinearity of the dependence of the potential vorticity (PV) on the streamfunction in the trapped-fluid area of the modon, i.e. where the streamlines are closed. The linearity of this dependence and the circularity of the trapped-fluid area are shown to be equivalent properties of a modon. Special attention is given to elliptical modons – extended both in the direction of the modon propagation and in the orthogonal direction, the baroclinic PV component being assumed continuous. The differences between the two types of elliptical modons are discussed. The simplest vortical couples and shielded modons are considered. In the context of the continuity of the baroclinic PV field, the stability of modons is discussed based on numerical simulations.

1. Introduction

Modons arise from Lamb's (1895, 1906) solution of the two-dimensional Euler equations (it is also valid for the f-plane). (In a historical essay, Meleshko & van Heijst (1994) noted that Chaplygin (1903) independently suggested the same solution.) On the barotropic β-plane, Stern (1975) and Larichev & Reznik (1976) constructed a standing and a travelling modon solution, respectively. In all these solutions the modon is a dipole (or, more generally, an antisymmetric structure); its trapped-fluid area – the interior domain, in which the streamlines considered in the travelling frame are closed – is circular. Within and outside the circular separatix demarcating the two domains, two different linear relationships between potential vorticity (PV) and the streamfunction $\Psi = \psi + Uy$ hold, where ψ and Ψ designate the streamfunctions in the absolute and travelling coordinate frames, respectively, U the modon translation speed, and y the northward coordinate (x denotes the zonal coordinate).

The two-layer modons of Flierl *et al.* (1980) and the modon solutions that can be fitted to any continuous stratification (Kizner 1984, 1997) inherit these characteristics: the boundary of the region of closed streamlines is a circle (circular cylinder), and the PV vs. Ψ dependence in each layer (or at any level) is piecewise-linear. Similarly, three-dimensional spherical modons in a continuously (and linearly) stratified fluid are marked by linearity of the PV vs. Ψ relation (Berestov 1979; Kizner 1988).

The existence of nonlinear (in the above sense) modons was first reported by McWilliams & Zabusky (1982): in one of their numerical experiments, two merging Larichev–Reznik dipoles created a quasi-stationary vortex with a nonlinear interior relationship. Hesthaven *et al.* (1995) obtained a quasi-stationary dipolar nonlinear modon as an ultimate state of the evolution of some other nonlinear vortex solution of the two-dimensional Euler equations. In the both cases the form of the trapped-fluid domain of the modon was not analysed. Using asymptotic techniques Nycander (1988) suggested dipolar and quasi-monopolar nonlinear modon solutions with separatrices different from circles. The emergence of nonlinear barotropic dipoles from different initial conditions (including linear modons) was also observed in both numerical and laboratory experiments in the presence of viscosity (Nielsen & Juul Rasmussen 1997; van Geffen & van Heijst 1998). On the other hand, there is some evidence that with weak viscosity barotropic modons on the β-plane may keep their linearity for times exceeding the characteristic time scale (defined as the ratio of the modon radius and translation speed) even if initiated as f-plane modons (Sutyrin *et al.* 1994) or if resulting from the collapse of strongly unstable linear shielded β-plane modons (Kizner & Berson 2000).

An important step in the study of 'nonlinear' modons was made by Boyd & Ma (1990), who extended Lamb's theory by constructing numerically a stationary elliptical dipole. They considered only the ellipses extended in the direction of the modon propagation and revealed the specific nonlinear dependence between vorticity and Ψ characteristic of the interior domains of such ellipses.

Morel & McWilliams (1997) observed the emergence of nonlinear vortical structures in a baroclinic quasi-geostrophic (QG) model with high vertical resolution. In our recent two-layer numerical experiments (β-plane, equal-depth layers), at a certain stage of evolution circular modons sometimes switch to an oval (nearly elliptical) state, whose characteristic properties are nonlinearity of the interior PV vs. Ψ relationship and a saddle-like topography of the baroclinic mode (Kizner, Berson & Khvoles 2002, referred to below as KBK). Such modons have much in common with hetons (Hogg & Stommel 1985; Gryanik 1983, 1988) because their translation mechanism is due to oppositely signed vortices occurring in different layers and separated by a certain distance in the y-direction. They appear to represent a quite general type of baroclinic QG equilibrium and, therefore, merit detailed analysis.

The main objective of the present paper is the development of a method for the direct numerical construction of stationary non-circular β-plane baroclinic modon solutions with nonlinear interior relationships between PV and Ψ. As noted by Boyd & Ma (1990), "The shape of the modon and relationship between the vorticity and the streamfunction are two factors which can be used to determine the modon solution, and only one of them is independent". Based on this principle we focus our efforts on the construction of two-layer modons on the β-plane specifying the form of the separatrix, while the PV vs. Ψ dependence is determined *a posteriori*. (Verkley 1993 constructed numerically 'nonlinear' barotropic solutions on a sphere using, in essence, the opposite approach.) In order to minimize the number of free parameters of the problem, we impose some symmetry restrictions on the solutions sought. In particular, only figures symmetrical about the x- and y-axes are considered. While the barotropic PV component is continuous everywhere in the (x, y)-plane, a jump discontinuity of the baroclinic PV on the separatrix is permitted (non-smooth modons), and the amplitude of the external baroclinic field can be specified arbitrarily. In principle, this amplitude, the modon translation speed and the size can be fitted so as to allow continuity of the baroclinic PV field (smooth modons).

In § 2, the mathematical formulation is considered in detail. A numerical method for solving the problem is described in § 3. Some results of its application (including accuracy estimates) are presented in § 4, where the focus is on smooth elliptical modons. The stability properties of the smooth and non-smooth modons are discussed in § 5 based on numerical simulations.

2. Mathematical formulation

2.1. *Governing equations*

Consider a two-layer QG model in which the unperturbed layer depths are equal and the bottom is flat (horizontal). We are interested in localized vortices that travel steadily in the zonal direction at a constant speed U without changing either their form or other characteristics. Such a vortex, when considered in a coordinate frame attached to the vortex centre, is stationary. In this frame the governing equations – the equations of PV conservation – are as follows:

$$J(\Psi_1, q_1) = 0, \quad J(\Psi_2, q_2) = 0, \tag{1}$$

where

$$\Psi_1 = \psi_1 + Uy, \quad \Psi_2 = \psi_2 + Uy, \tag{2}$$

$$q_1 = \Delta\psi_1 + \Lambda^2(\psi_2 - \psi_1) + \beta y, \quad q_2 = \Delta\psi_2 + \Lambda^2(\psi_1 - \psi_2) + \beta y. \tag{3}$$

In equations (1)–(3) subscripts 1 and 2 are indices of the upper and lower layers, respectively; q_1 and q_2 are the PV in the layers; $\Lambda^2 = f_0^2\rho_0/(gh\delta\rho) = 2/L_{Ro}^2$, where $L_{Ro} = \sqrt{g\delta\rho H/(\rho_0 f_0^2)}$ is the internal Rossby radius, $H = 2h$ is the total depth of the fluid (h is the unperturbed layer depth), g is the acceleration due to gravity, ρ_0 and $\delta\rho$ are the mean density and the density jump between the layers; and f_0 and β are, respectively, the reference value of the Coriolis parameter f and the northward gradient of f (see, for example, Kamenkovich, Koshlyakov & Monin 1986, Ch. 2).

It is well-known that equations (1) imply the existence of some dependences between q_1 and Ψ_1, on the one hand, and q_2 and Ψ_2, on the other:

$$q_1 = F_1(\Psi_1), \quad q_2 = F_2(\Psi_2). \tag{4}$$

Moreover, in the exterior domain – on the open isolines of the streamfunctions Ψ_1 and Ψ_2 – these dependences are simple proportions (Flierl *et al.* 1980):

$$q_1 = l^2\Psi_1, \quad q_2 = l^2\Psi_2, \quad l^2 = \frac{\beta}{U}. \tag{5}$$

Finally, it is known (Larichev & Reznik 1976; Flierl *et al.* 1980) that a localized solution to equations (1)–(3) can exist only if $U \geqslant 0$. Below we shall see that, in the interior domain, i.e. within the trapped-fluid area, the functions F_1 and F_2 are determined by the shape of this area along with the translation speed and another independent parameter – the exterior baroclinic mode amplitude.

To give an exact formulation of the problem it is appropriate to rewrite the above model in terms of the barotropic (BT) and baroclinic (BC) modes that, in the equal-depth case, are defined as follows:

$$\psi_{BT} = \tfrac{1}{2}(\psi_1 + \psi_2), \quad \psi_{BC} = \tfrac{1}{2}(\psi_1 - \psi_2), \tag{6}$$

$$\Psi_{BT} = \tfrac{1}{2}(\Psi_1 + \Psi_2) = \psi_{BT} + Uy, \quad \Psi_{BC} = \tfrac{1}{2}(\Psi_1 - \Psi_2) = \psi_{BC}, \tag{7}$$

$$q_{BT} = \Delta\Psi_{BT} + \beta y = \Delta\psi_{BT} + \beta y, \quad q_{BC} = \Delta\Psi_{BC} - m^2\Psi_{BC} = \Delta\psi_{BC} - m^2\psi_{BC}, \tag{8}$$

where $m^2 = 2\Lambda^2$. The governing equations for the modes then are

$$J(\Psi_{BT}, q_{BT}) + J(\Psi_{BC}, q_{BC}) = 0, \tag{9}$$

$$J(\Psi_{BT}, q_{BC}) + J(\Psi_{BC}, q_{BT}) = 0. \tag{10}$$

2.2. *Symmetry restrictions*

The integral angular momentum of a localized solution to equations (9), (10) is zero (Flierl, Stern & Whitehead 1983), so that

$$\int\int \psi_{BT}\, \mathrm{d}x\, \mathrm{d}y = 0,$$

where the integration is performed over the whole (x, y)-plane. Therefore, vortices with a dipolar barotropic mode play a distinctive role in geophysical fluid dynamics. In an equal-depth two-layer QG model, the antisymmetry of the barotropic mode and symmetry of the baroclinic mode about the x-axis are conserved if they are present in the initial condition (KBK). Moreover, our experiments on the evolution of circular modons tilted at 30° to the x-axis suggest that, when asymmetrically perturbed, modons in such a model tend to stabilize in the states in which the asymmetric components in Ψ_{BT} and Ψ_{BC} are negligible (KBK). This explains our particular interest in searching here for the solutions to equations (9), (10) categorized by antisymmetry about the x-axis and symmetry about the y-axis of the barotropic mode, and the symmetry of the baroclinic mode about both the x- and y-axes.

Thus we assume that

$$\Psi_{BT}(x, -y) = -\Psi_{BT}(x, y), \quad \Psi_{BT}(-x, y) = \Psi_{BT}(x, y), \tag{11}$$

$$\Psi_{BC}(-x, y) = \Psi_{BC}(x, -y) = \Psi_{BC}(-x, -y) = \Psi_{BC}(x, y). \tag{12}$$

Clearly, in this case, the functions ψ_1 and ψ_2, as well as Ψ_1 and Ψ_2, are mutually antisymmetric:

$$\psi_1(x, -y) = -\psi_2(x, y), \quad \Psi_1(x, -y) = -\Psi_2(x, y). \tag{13}$$

We shall assume for simplicity that in both layers, a common separatrix Γ demarcates the exterior region, where the proportions (5) hold, and the interior domain, where the relationships (4) differ from (5). It readily follows from (13) that Γ must be symmetric about both the x- and y-axes. In addition, we shall regard the periodic function $r = r_\Gamma(\theta)$ determining the closed contour Γ to be smooth and single-valued. The solutions presented below in § 4 correspond to the particular case of smooth convex contours Γ that deviate moderately from a circle.

Consider two symmetrical points (x_0, y_0) and $(x_0, -y_0)$ on the contour Γ. Since Γ is a streamline (in the travelling coordinate frame), i.e. $\Psi_1|_\Gamma = \text{const}$, we have

$$\Psi_1(x_0, y_0) = \Psi_1(x_0, -y_0).$$

Due to (11), (12), this is possible only if

$$\Psi_{BT}(x_0, y_0) = \Psi_{BT}(x_0, -y_0) = 0.$$

In other words, at the contour Γ the following equalities hold:

$$\Psi_{BT}|_\Gamma = 0, \quad \Psi_{BC}|_\Gamma = \text{const}. \tag{14}$$

2.3. *Exterior problem*

The equations that determine the barotropic and baroclinic modes in the exterior region, $r > r_\Gamma(\theta)$, follow from (5) and (8); these are Helmholtz equations:

$$\Delta\psi_{BT}^{(Ex)} - l^2\psi_{BT}^{(Ex)} = 0, \quad \Delta\psi_{BC}^{(Ex)} - (l^2 + m^2)\psi_{BC}^{(Ex)} = 0, \tag{15}$$

where superscript (Ex) is used to distinguish the exterior solution from the interior one. The boundary conditions that complete the formulation of the exterior problem follow from (14) and the fact that the solution we are looking for is localized:

$$\left(\psi_{BT}^{(Ex)} + Uy\right)\big|_\Gamma = 0, \quad \psi_{BC}^{(Ex)}\big|_\Gamma = C, \tag{16}$$

$$\psi_{BT}^{(Ex)} \to 0, \quad \psi_{BC}^{(Ex)} \to 0 \quad \text{as} \quad r \to \infty. \tag{17}$$

Hereinafter the translation speed $U > 0$ is assumed to be fixed; C is an arbitrary constant unless otherwise specified; $r = \sqrt{x^2 + y^2}$ and θ are polar coordinates; conditions (17) should be read so that the functions $\psi_{BT}^{(Ex)}$ and $\psi_{BC}^{(Ex)}$ go to zero exponentially.

We represent a solution to equations (15) that satisfies conditions (17) and the above symmetry/antisymmetry restrictions in the following form (Flierl *et al.* 1980):

$$\psi_{BT}^{(Ex)} = \sum_{i=0}^{\infty} A_{2i+1} K_{2i+1}(lr) \sin[(2i+1)\theta], \tag{18}$$

$$\psi_{BC}^{(Ex)} = \sum_{i=0}^{\infty} B_{2i} K_{2i}(r\sqrt{l^2 + m^2}) \cos(2i\theta), \tag{19}$$

where K_ν is the ν-order modified Bessel (Macdonald) function. The natural domain of convergence of the Fourier–Bessel series (18), (19) is the exterior of a circle, while for a non-circular separatrix, the domain of convergence needs to be the circle of smallest radius that touches any part of Γ. The latter is not guaranteed for an arbitrary contour (Boyd 2002), but can be expected to hold when Γ is smooth and convex to such a degree that it deviates moderately from a circle. In any case, once the exterior solution is based on the expansions (18), (19), it should *be a posteriori* checked for regularity in the domain bounded by Γ and the smallest circle enclosing Γ. All the solutions presented in §§ 4 and 5 were tested and proved to be regular (see §§ 3.1 and 4.3). In § 3.3, a more general, rigorous approach free of the above restraint is presented that can also be extended to constructing modons with different separatrices in the upper and lower layers.

Given the contour Γ and constant C, the coefficients A_{2i+1} and $B_{2i} (i \geqslant 0)$ are completely determined via conditions (16), where the variable y is replaced with $r\sin\theta$. The uniqueness of this determination follows from the fact that the exterior Dirichlet problem (16), (17) for the Helmholtz equations (15) is always solvable, yielding a unique solution (Koshliakov, Gliner & Smirnov 1962, Ch. 25), and that, at any fixed r, the Fourier decompositions (18) and (19) are also unique.

If, for example, Γ is a circle of a radius a, one obtains

$$A_1 = -\frac{aU}{K_1(la)}, \quad B_0 = \frac{C}{K_0(a\sqrt{l^2 + m^2})}, \tag{20}$$

$$A_{2i+1} = B_{2i} = 0 \quad \text{for} \quad i > 0. \tag{21}$$

Hence we can conclude that, in circular modons, the external barotropic field necessarily contains only one azimuthal harmonic

$$\psi_{BT}^{(Ex)} = \frac{aU}{K_1(la)} K_1(lr)\sin\theta, \tag{22}$$

whereas the baroclinic mode can only be radially symmetric:

$$\psi_{BC}^{(Ex)} = \frac{C}{K_0(a\sqrt{l^2+m^2})} K_0(r\sqrt{l^2+m^2}) \tag{23}$$

(cf. Flierl *et al.* 1980; and Reznik & Sutyrin 2001, where these restrictions were postulated).

If Γ is non-circular the exterior barotropic mode may, generally, comprise all the odd azimuthal harmonics ($\sin[(2i+1)\theta], i \geqslant 0$), and the baroclinic mode all the even harmonics ($\cos(2i\theta), i \geqslant 0$). For example, this is the case when Γ is an ellipse. We emphasize that, as seen from (16), (19), once U and Γ are given, the baroclinic mode of the exterior solution is determined only to an arbitrary factor C.

2.4. *Interior problem*

In this subsection, contour Γ is assumed to be fixed. To set up the interior problem (at $r < r_\Gamma(\theta)$), we supplement equations (9), (10) with the following boundary conditions:

$$\Psi_{BT}|_\Gamma = 0, \quad \Psi_{BC}|_\Gamma = C, \tag{24}$$

$$\frac{\partial}{\partial n}\Psi_{BT}|_\Gamma = \frac{\partial}{\partial n}\Psi_{BT}^{(Ex)}\big|_\Gamma, \quad \frac{\partial}{\partial n}\Psi_{BC}|_\Gamma = \frac{\partial}{\partial n}\Psi_{BC}^{(Ex)}\big|_\Gamma, \tag{25}$$

where the differentiation is carried out in the direction of the (external) normal $\boldsymbol{n}$ to the contour Γ. Conditions (24), (25) require the continuity of the streamfunction (pressure) and velocity fields at the separatrix. An analogy with the classical linear problems of mathematical physics suggests that these conditions are sufficient for the correctness of the interior problem once we confine ourselves to regular solutions. This is supported by the results presented in § 4 and discussed in the Conclusion.

Let us now clear up the question of the continuity of the barotropic and baroclinic PV fields at the separatrix Γ. Based on (4) and (5), in a manner similar to that in which relationships (14) were obtained, we arrive at the conclusion that $q_{BT}|_\Gamma = q_{BT}^{(Ex)}|_\Gamma = 0$. Thus, the barotropic PV component in the solution of the problem (9), (10), (24), (25) is continuous. The same cannot be said of the baroclinic PV mode: generally, there is a jump in q_{BC} values across the contour Γ. However, both the exterior and interior baroclinic PV assume constant values at Γ:

$$q_{BC}^{(Ex)}\big|_\Gamma = l^2 C, \quad q_{BC}|_\Gamma = F_1(\Psi_{BC}|_\Gamma) = F_1(C).$$

Formally, solutions with a jump in q_{BC} at Γ, i.e. those in which $F_1(C) \neq l^2 C$, are legitimate as Γ is both a streamline and a material contour (pathway of fluid particles), and hence equations (9), (10) are satisfied at Γ.

The presence of one degree of freedom in the problem (9), (10), (24), (25), that is, of an arbitrary constant C, allows us to pose the question of the existence of high-smoothness solutions, i.e. those in which q_{BC} is continuous at Γ. To provide the continuity of the baroclinic PV field, parameter C must obey the equation

$$F_1(C) - l^2 C = 0. \tag{26}$$

In this case C must be a function of U. There are grounds to believe that, on the β-plane, solutions marked by a discontinuity of the baroclinic PV are unstable,

whereas stable configurations are smooth (see § 5). Therefore, below in § 4 we present such solutions that satisfy condition (26), referring to them as *smooth* ones.

3. Numerical method

In the general case, solving the interior problem analytically is hardly possible due to its essential nonlinearity. A method will be presented here that allows the construction of numerical solutions at quite a high accuracy for symmetric contours Γ.

3.1. *Exterior problem*

In order to evaluate the exterior solution we truncate the series (18), (19), i.e. fix some integer $N \geqslant 0$ and put

$$A_{2i+1} = B_{2i} = 0 \quad \text{for} \quad i > N. \tag{27}$$

In most practical computations N was taken equal to 11, i.e. 24 azimuthal harmonics were left (12 odd and 12 even).

Next, we choose $P > N+1$ points $(r_{\Gamma,j}, \theta_j)$ distributed along Γ in the first quadrant $(0 < \theta \leqslant \pi/2)$ and, at every pair $(r_{\Gamma,j}, \theta_j)$, substitute expansions (18), (19), (27) in (16). This yields

$$\sum_{i=0}^{N} A_{2i+1} K_{2i+1}(l r_j) \sin[(2i+1)\theta_j] = -U r_{\Gamma,j} \sin\theta_j, \tag{28}$$

$$\sum_{i=0}^{N} B_{2i} K_{2i}(\sqrt{l^2+m^2}\, r_j) \cos(2i\theta_j) = C, \tag{29}$$

where $j = 1, \ldots, P$ is the point index.

Relationships (28), (29) represent two independent linear systems in A_{2i+1} and B_{2i}. The number of equations in each of these systems, P, exceeds that of the unknowns, $N+1$. If P is sufficiently large (compared to $N+1$), then non-zero $(N+1)\times(N+1)$ minors can be found in each of the matrices of systems (28) and (29), which guarantees the uniqueness (and reliability) of the solution to (28) and (29) in the least squares (LSQ) sense. Another advantage of solving an over-determined problem is a guarantee that the exterior field based on truncated series will provide a good approximation to conditions (16) everywhere along Γ. In calculations for elliptical figures (most of the results presented below) P was taken to be 300.

The possibility of representing the exterior solution in the form (18), (19) can be validated by testing the ability of these series to satisfy conditions (16). Clearly, the stronger the deviation of the contour Γ from a circle, the more harmonics must be taken to represent the exterior solution. On the other hand, one could anticipate that, as the boundary becomes more and more different from a circle, the numerical determination of the coefficients A_{2i+1} and B_{2i} in (28), (29) might eventually become ill-conditioned (due to the problem of the domain of convergence discussed in § 2.3) resulting in the error in fulfillment of (16) not continuing to decrease monotonically with increasing N. According to our tests, when dealing with elliptical modons and moderate translation speeds ($U \sim 0.1$ to 1.5), the series representation (18), (19) of the exterior field (outside Γ) is valid at least for ellipses with aspect ratios up to 2:1, in which case 50 azimuthal harmonics ($N = 24$) were used. We note that this specific limitation was conditioned by the limited precision in computing the modified Bessel functions provided by the software used.

3.2. *Interior problem*

3.2.1. *Successive linearization scheme*

To solve the interior problem we adopt the successive linearization procedure – a version of the Newton–Kantorovich method (Kantorovich 1948). The iteration process underlying this approach is as follows:

Let IT be the iteration index ($IT = 0, 1, \ldots$). Once the ITth approximation, $\Psi_{BT}^{(IT)}$, $\Psi_{BC}^{(IT)}$, is known, the next, $(IT+1)$th approximation is given by

$$\Psi_{BT}^{(IT+1)} = \Psi_{BT}^{(IT)} + \delta_{BT}, \quad \Psi_{BC}^{(IT+1)} = \Psi_{BC}^{(IT)} + \delta_{BC}, \tag{30}$$

$$q_{BT}^{(IT+1)} = q_{BT}^{(IT)} + \Delta\delta_{BT}, \quad q_{BC}^{(IT+1)} = q_{BC}^{(IT)} + \Delta\delta_{BC} - m^2\delta_{BC}, \tag{31}$$

where the corrections δ_{BT} and δ_{BC} satisfy the third-order linear differential equations

$$J\left(\delta_{BT}, q_{BT}^{(IT)}\right) + J\left(\Psi_{BT}^{(IT)}, \Delta\delta_{BT}\right) + J\left(\delta_{BC}, q_{BC}^{(IT)}\right) + J\left(\Psi_{BC}^{(IT)}, \Delta\delta_{BC} - m^2\delta_{BC}\right)$$
$$= -J\left(\Psi_{BT}^{(IT)}, q_{BT}^{(IT)}\right) - J\left(\Psi_{BC}^{(IT)}, q_{BC}^{(IT)}\right), \tag{32}$$

$$J\left(\delta_{BT}, q_{BC}^{(IT)}\right) + J\left(\Psi_{BT}^{(IT)}, \Delta\delta_{BC} - m^2\delta_{BC}\right) + J\left(\delta_{BC}, q_{BT}^{(IT)}\right) + J\left(\Psi_{BC}^{(IT)}, \Delta\delta_{BT}\right)$$
$$= -J\left(\Psi_{BT}^{(IT)}, q_{BC}^{(IT)}\right) - J\left(\Psi_{BC}^{(IT)}, q_{BT}^{(IT)}\right). \tag{33}$$

These equations are supplemented by the following boundary conditions:

$$\delta_{BT}|_{\Gamma} = -\Psi_{BT}^{(IT)}\big|_{\Gamma}, \quad \frac{\partial}{\partial n}\delta_{BT}|_{\Gamma} = \frac{\partial}{\partial n}\Psi_{BT}^{(Ex)}\big|_{\Gamma} - \frac{\partial}{\partial n}\Psi_{BT}^{(IT)}\big|_{\Gamma}, \tag{34}$$

$$\delta_{BC}|_{\Gamma} = C - \Psi_{BC}^{(IT)}\big|_{\Gamma}, \quad \frac{\partial}{\partial n}\delta_{BC}|_{\Gamma} = \frac{\partial}{\partial n}\Psi_{BC}^{(Ex)}\big|_{\Gamma} - \frac{\partial}{\partial n}\Psi_{BC}^{(IT)}\big|_{\Gamma}. \tag{35}$$

Formally, (30), (31), (34) and (35) imply that, starting from the second iteration, the current corrections satisfy the conditions

$$\delta_{BT}|_{\Gamma} = \frac{\partial}{\partial n}\delta_{BT}|_{\Gamma} = 0, \quad \delta_{BC}|_{\Gamma} = \frac{\partial}{\partial n}\delta_{BC}|_{\Gamma} = 0.$$

Nevertheless, because the problem is solved numerically, we use the boundary conditions for the corrections in the form (34), (35) to provide the maximal available accuracy.

The iterative procedure (30)–(35) converges to the true solution of the problem (9), (10), (24), (25) if the initial guess ($\Psi_{BT}^{(0)}$ and $\Psi_{BC}^{(0)}$) is chosen sufficiently close to this solution (Kantorovich 1948).

3.2.2. *Initial guess*

The procedure of constructing the initial guess, $\Psi_{BT}^{(0)}$, $\Psi_{BC}^{(0)}$, consists of several steps. We start with the construction of a circular modon solution (characterized by a piecewise linear PV vs. Ψ relationship) taking as its radius the mean radius $r_0 = r_0(\Gamma) = \sqrt{S_\Gamma}$ of the contour Γ (where S_Γ is the area bounded by Γ) and taking C as the boundary value of Ψ_{BC}. As parameters U and r_0 are not especially suited to provide the continuity of q_{BC} at $r = r_0$ (Kizner 1997; KBK), the resulting circular modon is a general-type 'modon with a rider' described by Flierl *et al.* (1980); its analogue in the classical two-dimensional fluid dynamics is the 'non-symmetrical dipole' of Chaplygin (1903) reproduced and analysed by Meleshko & van Heijst (1994). We then stretch or contract the fields Ψ_{BT} and Ψ_{BC} in the radial directions so as to fulfil the conditions $\Psi_{BT} = 0$ and $\Psi_{BC} = C$ at the contour Γ. Finally, the obtained

Ψ_{BT} field is approximated by a $(2N+1)$-degree polynomial in x, y, which is even in x and odd in y, and the Ψ_{BC} field is approximated by a $2N$-degree polynomial, which is odd in both x and y.

When examining the possible PV vs. Ψ relationships for circular modons (see below, §4.1) we experiment with initial guesses different from the exact circular solution. To set such an initial guess, we use an inverse procedure starting from numerically determined elliptical (and some other) solutions and adapting them to a circle by stretching/compressing.

3.2.3. *Determining the corrections*

At this stage, a collocation method is used. The corrections δ_{BT} and δ_{BC} are represented as polynomials of the same degrees as the initial guess:

$$\delta_{BT} = \sum_{0 \leqslant p+s \leqslant N} \alpha_{p,s}^{(BT)} x^{2p} y^{2s+1}, \quad \delta_{BC} = \sum_{0 \leqslant p+s \leqslant N} \alpha_{p,s}^{(BC)} x^{2p} y^{2s}. \tag{36}$$

Now that the functions $\Psi_{BT}^{(0)}$, $\Psi_{BC}^{(0)}$, δ_{BT} and δ_{BC} are given in polynomials, all differential operators appearing in equations and conditions (30)–(35) can be expressed explicitly, and the problem, which is solved at every iteration, is reduced to the determination of the coefficients $\alpha_{p,s}^{(BT)}$ and $\alpha_{p,s}^{(BC)}$ appearing in (36). Note that the polynomial approximation ensures regularity of the solution (in the case that the iterative process converges). For some special types of figures, orthogonal mapping and collocation methods based on a linear combination of products of Chebyshev polynomials in the resulting rectangular domain can be used (Boyd 2001).

Symmetry/antisymmetry of the modes allows us to consider only one quarter of the (x, y)-plane when evaluating the coefficients $\alpha_{p,s}^{(BT)}$ and $\alpha_{p,s}^{(BC)}$. At the first stage of computations we choose the first quadrant ($x \geqslant 0$, $y > 0$), coat it with a rectangular mesh and consider a grid domain Ω bounded by the straight lines $x = 0$, $y = 0$ and the contour Γ. We then consider equations (32), (33) at each grid point belonging to Ω, thus obtaining a system of $2K$ linear equations in $\alpha_{p,s}^{(BT)}$ and $\alpha_{p,s}^{(BC)}$, where $K \gg N$ is the total number of grid points in domain Ω. In a similar way, we obtain another system of $6P$ linear equations in $\alpha_{p,s}^{(BT)}$ and $\alpha_{p,s}^{(BC)}$ by considering equations (32), (33) and conditions (34), (35) at each jth point belonging to the contour Γ and used above to determine the coefficients A_{2i+1} and B_{2i} in (28), (29). We then have a system of $2K + 6P$ equations in $(N+1)(N+2)$ unknowns and solve it in the LSQ sense, which is possible because $2K + 6P \gg (N+1)(N+2)$. To avoid dealing with small or large numbers, the variables x and y are scaled by r_0.

Once the approximate solution based on a regular collocation is found, we change the grid by making it denser in the vicinity of the poles of the barotropic and baroclinic PV fields, and rerun the iterative procedure starting it from the approximation found. It should be noted that taking the number of mesh points (and thus the number of equations) to be larger than the number of unknowns pursues two goals: it ensures that the linear system in $\alpha_{p,s}^{(BT)}$ and $\alpha_{p,s}^{(BC)}$ is well-determined and provides a good (in the above LSQ sense) polynomial approximations to the true exact solution everywhere in Ω by damping the possible 'high-frequency' oscillations of the polynomials.

The number of computations increases considerably when a modon solution with a smooth baroclinic PV is sought, because in this case the procedure described above is embedded within a loop to determine the constant C satisfying equation (26).

The results presented below in §4 were obtained using the mesh size $h \approx r_0/30$, i.e. for $K \approx 700$. The iterative procedure was assumed to be converged when the relative change in the sum (over all $2K + 6P \approx 3200$ equations) of squared residuals became

smaller than a given tolerance level (usually 10^{-3} to 10^{-4}). The accuracy of the method is considered in § 4.3.

3.3. *Generalization*

When the separatrix Γ deviates strongly from a circle (see § 2.3), the construction of the exterior solution can be facilitated by introducing an additional circular contour $r = R$ enclosing the contour Γ. This 'false' boundary will be denoted by Γ_R, and the symbols $\Psi_{BT}^{(Ex)}$ and $\Psi_{BC}^{(Ex)}$ will be allotted to the exterior solution outside Γ_R only. The solution at $r \geqslant R$ can always be sought in the series form (18), (19) since these series converge everywhere on Γ_R and outside it. By introducing Γ_R we obtain an intermediate domain bounded by the contours Γ and Γ_R (generally, this domain may break down into a number of simply connected domains). The solution corresponding to this domain, called intermediate and denoted as $\psi_{BT}^{(Im)}$, $\psi_{BC}^{(Im)}$, satisfies the equations

$$\Delta\psi_{BT}^{(Im)} - l^2\psi_{BT}^{(Im)} = 0, \quad \Delta\psi_{BC}^{(Im)} - (l^2 + m^2)\psi_{BC}^{(Im)} = 0, \tag{37}$$

and obeys the boundary conditions

$$\left(\psi_{BT}^{(Im)} + Uy\right)\big|_{\Gamma} = 0, \quad \psi_{BC}^{(Im)}\big|_{\Gamma} = C \tag{38}$$

that replace (16). In addition (if a smooth solution outside the contour Γ exists) the intermediate solution must match smoothly the series solution (18), (19) at the circle Γ_R so as to comply with the following conditions:

$$\Psi_{BT}^{(Im)}\big|_{\Gamma_R} = \Psi_{BT}^{(Ex)}\big|_{\Gamma_R}, \quad \Psi_{BC}^{(Im)}\big|_{\Gamma_R} = \Psi_{BC}^{(Ex)}\big|_{\Gamma_R}, \tag{39}$$

$$\frac{\partial}{\partial n}\Psi_{BT}^{(Im)}\bigg|_{\Gamma_R} = \frac{\partial}{\partial n}\Psi_{BT}^{(Ex)}\bigg|_{\Gamma_R}, \quad \frac{\partial}{\partial n}\Psi_{BC}^{(Im)}\bigg|_{\Gamma_R} = \frac{\partial}{\partial n}\Psi_{BC}^{(Ex)}\bigg|_{\Gamma_R}. \tag{40}$$

Finally, as the interior solution borders the intermediate one, conditions (25) must be replaced with the following:

$$\frac{\partial}{\partial n}\Psi_{BT}|_{\Gamma} = \frac{\partial}{\partial n}\Psi_{BT}^{(Im)}\big|_{\Gamma}, \quad \frac{\partial}{\partial n}\Psi_{BC}|_{\Gamma} = \frac{\partial}{\partial n}\Psi_{BC}^{(Im)}\big|_{\Gamma}. \tag{41}$$

In (40) and (41), the symbol $\partial/\partial n$ designates the derivative in the direction normal to Γ_R and Γ, respectively. It is straightforward to show that conditions (39), (40) guarantee the smoothness of the functions $q^{(BT)}$ and $q^{(BC)}$ on Γ_R.

Because of the interdependence of the exterior and intermediate solutions, equations and conditions (18), (19), (37)–(40) must be solved simultaneously within the same numerical procedure. At this stage, to evaluate the intermediate solution, we again use the collocation method and polynomial approximation. The resulting two independent linear systems in the polynomial and Fourier–Bessel coefficients – one for the barotropic mode and the other for the baroclinic mode – are solved in the LSQ sense.

This general scheme is especially appropriate for strongly curved contours. In the present work, where we focus manly on moderately elliptical modons, it was used for selective checking of the solutions found with the 'simple' technique described in §§ 3.1 and 3.2. In all cases the results obtained using the two methods were practically identical.

4. Applications

4.1. *Circularity and linearity*

As ascertained above, in a circular modon the barotropic and baroclinic modes of the exterior solution can contain only one gravest azimuthal harmonic each (see equations (20)–(23)). The familiar analytical circular solution with a linear interior PV vs. Ψ dependence in the layers (Flierl *et al.* 1980) contains the same gravest azimuthal harmonics in the interior domain and, obviously, obeys conditions (24), (25). This fact suggests that linearity of the interior PV vs. Ψ dependence is intrinsic in circular solutions only. This statement was verified by computations and proved to be correct (figures 1–3).

To verify that, in a circular modon, the PV vs. Ψ relation is always linear we started the iterative procedure from various initial guesses which, in turn, were obtained using previously computed nonlinear (mostly elliptical) numerical solutions. Whenever the process converged, the resulting interior solution was linear to an extremely high accuracy almost independently of N (which varied from 7 to 15) and the corresponding values of h and P (see § 4.3). This allows us to conclude that circular baroclinic modons are always 'linear'. Assuming this as a proven fact, one must accept that the analytical solution with a continuous baroclinic PV field is the only possible circular baroclinic modon solution of such smoothness. We note that, in this particular case, conditions (24)–(26) are satisfied at arbitrary value of C, i.e. at any strength of the rider. They determine the 'dispersion relation' $r_0 = r_C(U)$ between the separatrix radius r_0 and the translation speed U of a circular modon: at a smaller or larger radius (for a given U) the baroclinic PV will necessarily experience a jump at the separatrix. An example of a smooth circular baroclinic solution obtained numerically is shown in figure 1; it is identical to the analytical solution, i.e. is composed of a barotropic Larichev–Reznik dipole and a smooth circularly symmetric baroclinic 'rider'; the layer PV vs. Ψ relation in the interior domain is linear in this modon (figure 3*a*). Circular modons that do not obey the smoothness condition (26) are considered in § 5. It should be noted that the interior q_1 vs. Ψ_1 relations shown here and below have been plotted as scatter-graphs based on our computations. They appear as solid lines due to the high resolution and accuracy of the numerical procedure applied (see also § 4.3).

The truth of the converse statement is confirmed by the experiments with non-circular figures. Computations show that any non-circularity of the separatrix results in nonlinearity of the interior solution. Even very small deviations of Γ from a circle may sometimes lead to considerable deformations of the PV field compared to the circular solution (figure 2), and the PV vs. Ψ scatter-diagram may become noticeably distorted (figure 3*b*). Here and below all the variables are non-dimensional, the scales being: L_{Ro} for the space variables x, y; βL_{Ro}^2 for U; βL_{Ro}^3 and βL_{Ro} for the streamfunction and PV, respectively.

4.2. *Smooth elliptical modons*

An ellipse, symmetrical about the x- and y-axes, is defined by two independent parameters. In order to comply with the parameterization of the oval modons applied in KBK, we shall use the aspect ratio r_y/r_x (or r_x/r_y) of the ellipse radii in the y- and x-directions and its mean radius $r_0 = \sqrt{r_x r_y}$. Clearly, if $r_y/r_x \neq 1$, three parameters U, r_0 and r_y/r_x completely determine a smooth baroclinic elliptical modon, the parameter C being a function of these – see equation (26). In our numerical evolution experiments (two-layer equal-depth model), transitions of circular modons to quasi-elliptical states

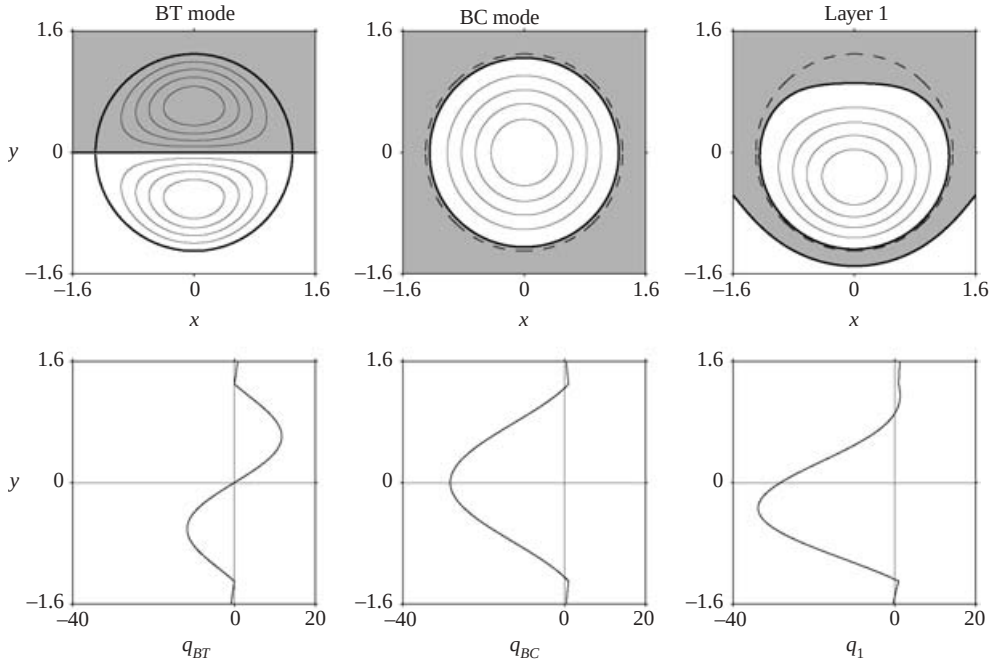

FIGURE 1. Potential vorticity fields of the smooth circular modon propagating at the speed $U = 0.7$ (the corresponding radius is $r_0 \approx 1.30$; $C = 0.675$): upper panel – contours of constant PV; lower panel – cross-sections at $x = 0$. The interval between the contours is 20% of the maximum; regions of positive values are shaded; dashed line, separatrix Γ.

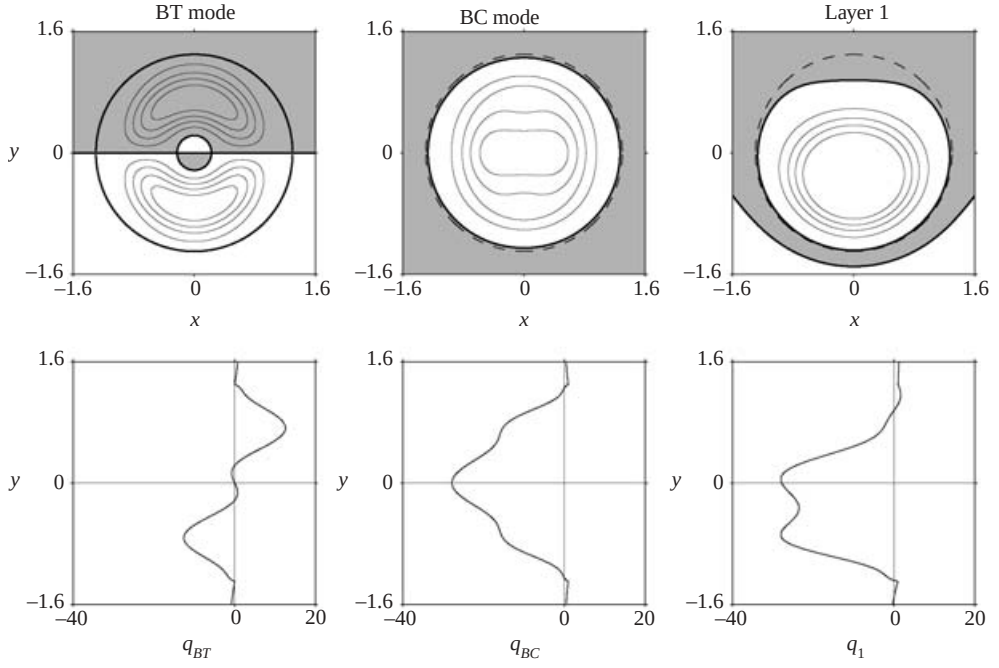

FIGURE 2. Potential vorticity fields in the smooth modon with a separatrix given by the equation $r = 1.30(1 + 0.005 \sin^2 2\theta)$; other parameters and notation (contours, shading, dashed line) as in figure 1.

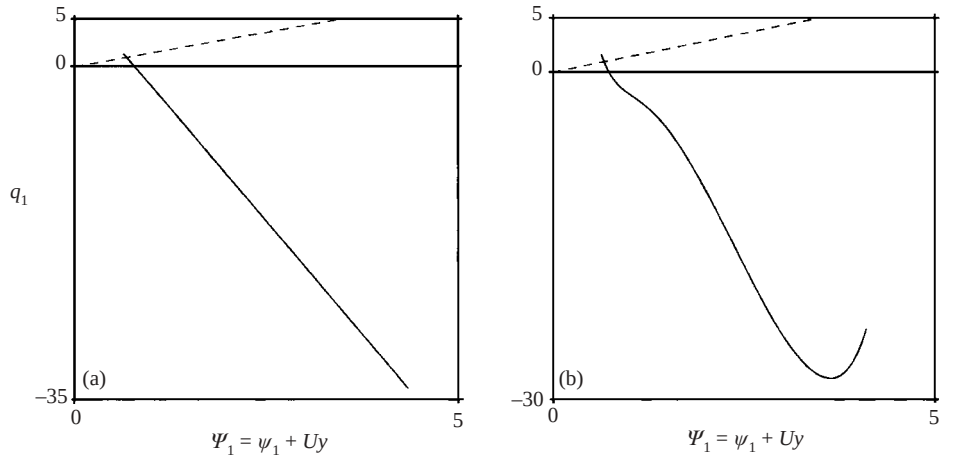

FIGURE 3. PV vs. Ψ scatter-graph for the upper layer: (*a*) circular modon shown in figure 1; (*b*) non-circular modon shown in figure 2. Solid line, interior domain; dashed line, exterior.

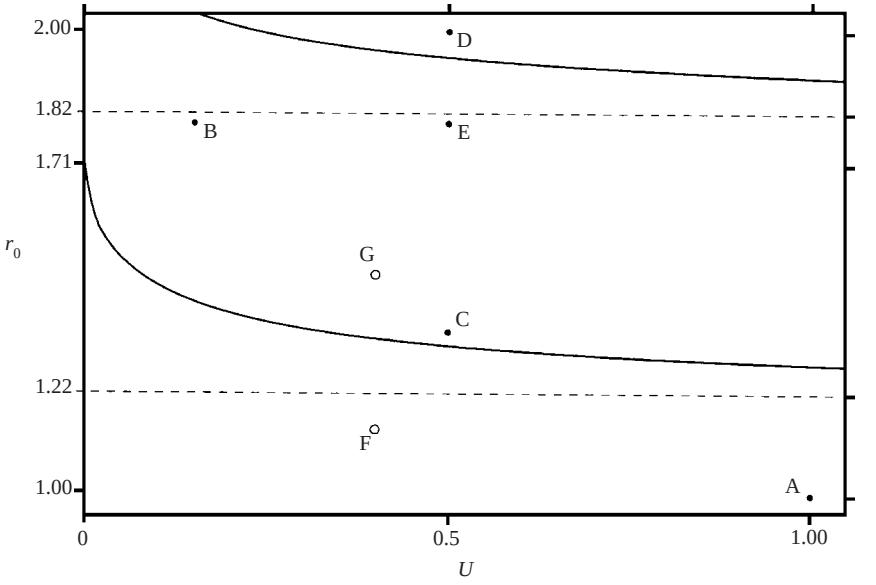

FIGURE 4. Regions of different types of modon solutions in the (U, r_0)-plane: solid lines, branches of the dispersion relationship $r_0 = r_0(U)$ for the smooth circular modons; dashed lines, their asymptotes; solid circles A to E, the modons shown in figures 5–11; open circles F, G, modons whose evolution is shown in figure 13.

with separatrices extended in the y-direction were observed (KBK). Therefore, such ellipses ($r_y/r_x > 1$) will be referred to as *ordinary*, while those extended in the x-direction ($r_x/r_y > 1$), will be referred to as *extraordinary*.

As noted above, in the particular case of smooth circular modons ($r_y/r_x = 1$), the radius r_0 is a function of the translation speed U. This function is multi-valued (solid lines in figure 4). The circular solutions corresponding to the lower branch have the simplest non-shielded structure – dipolar barotropic mode and monopolar baroclinic 'rider' (figure 1). The solutions corresponding to the higher branches belong to the

category of shielded modons: the barotropic mode in such solutions is four-polar. One might expect that the branches of the relation $r_0 = r_C(U)$ separate regions of different modon types in the $(r_0 U)$-plane. This appears to be generally true, with a correction for the fact that a full classification of elliptical modons can be performed by analysing the three-dimensional surface determined by the dispersion relation $r_0 = r_0(U, C, r_y/r_x)$ in a four-dimensional parameter space, whereas in the (r_0, U)-plane we are dealing only with a two-dimensional projection of this surface (see also KBK).

Beneath the lower branch of the relation $r_0 = r_C(U)$, only non-shielded ordinary elliptical solutions were found (e.g. point A in figure 4), while non-shielded extraordinary modons were found only above it, but not too close to the upper branch (e.g. point B in figure 4). On and above but close to the lower branch, apart from the extraordinary solutions, ordinary modons are present (e.g. point C in figure 4). The latter, however, possess some properties that differentiate them from the ordinary modons belonging to the domain $r_0 < r_C(U)$. In figures 5–8, the non-shielded elliptical modon solutions of different types are shown corresponding to points A–C in figure 4.

The characteristic feature of the ordinary elliptical modons found beneath the lower branch is the saddle-like shape of the baroclinic component, which can normally be observed in both the streamfunction and PV fields, but is more pronounced in the latter (figure 5). The bimodal character of the baroclinic PV distribution results, in each layer, in one of the baroclinic PV peaks nearly compensating the opposite-sign barotropic peak. This is apparent in the concentration of the positive and negative PV in different half-planes (with respect to the x-axis) and different layers (figure 5*b*). In other words, such a vortex structure represents essentially a distributed heton.

While the barotropic, baroclinic and layer streamfunction fields of the extraordinary modon (figure 6*a*) are roughly similar to those of a circular modon (cf. KBK), its PV fields exhibit a number of peculiarities (figure 6*b*). First, the barotropic PV field has small dents in the regions where the maximal and minimal values are assumed. Second, the central peak of the baroclinic PV is supplemented by two minor peaks in the interior domain. Accordingly, the layer PV distribution in the interior appears as two patches of nearly constant (though somewhat wavy) PV, opposite in sign, surrounded by rims of strong PV gradients.

The difference between the ordinary and extraordinary elliptical modons is manifested in specific features of their scatter-diagrams (figure 7). The solid lines in figures 7(*a*) and 7(*b*) that show the interior q_1 vs. Ψ_1 dependences are, in general, oppositely curved and, in the extraordinary modon, the graph has a volute on one of the ends, reflecting the dented character of the PV distribution in the area of its highest values.

Above the lower branch of the relationship $r_0 = r_C(U)$, in the larger ordinary modons, the internal baroclinic PV field may be single-modal or bimodal, depending on the modon translation speed and mean radius. Figure 8 represents an example of such an ordinary elliptical modon at $U = 0.5$ and $r_0 = 1.35$ with only one extremum in both the baroclinic streamfunction and PV fields. Correspondingly, the layer PV in the interior shows up as a single peak on a patch with a more or less homogeneous distribution (figure 8*b*). The shape of the interior scatter-graph of this solution is qualitatively similar to that of the 'small' ordinary modons (cf. figures 7*a* and 8*c*).

In the vicinity of the second branch of the relation $r_0 = r_C(U)$ these are shielded elliptical modons, but here ordinary modons are observed above this branch and extraordinary modons below it (points D, E in figure 4). The corresponding solutions are shown in figures 9–11. They look qualitatively similar to each other in terms of

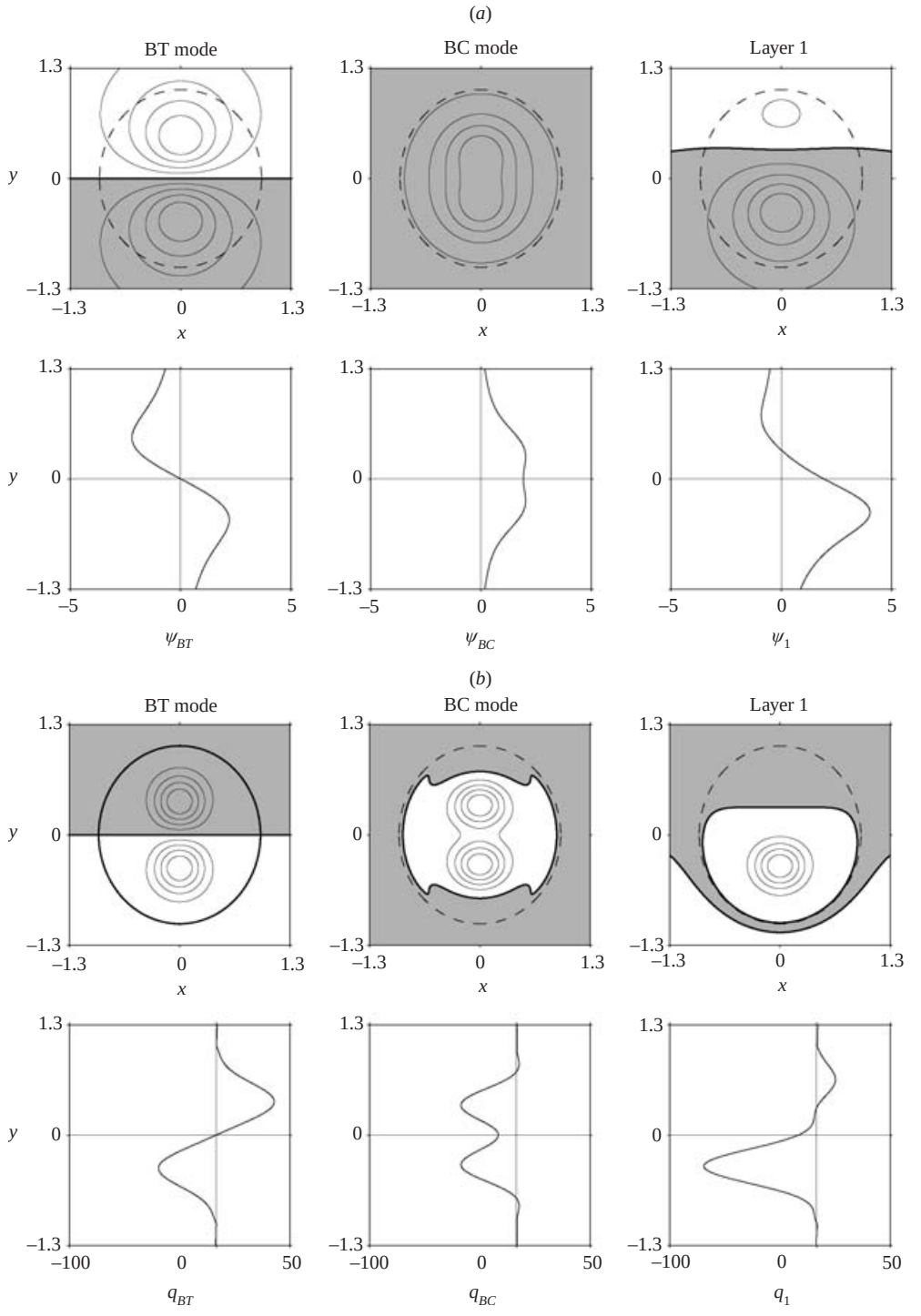

FIGURE 5. The ordinary elliptical modon given by the parameters $U = 1$, $r_0 = 1$, $r_y/r_x = 1.1$ and labelled A in figure 4: (*a*) streamfunction fields (ψ); (*b*) PV fields. Notation as in figure 1.

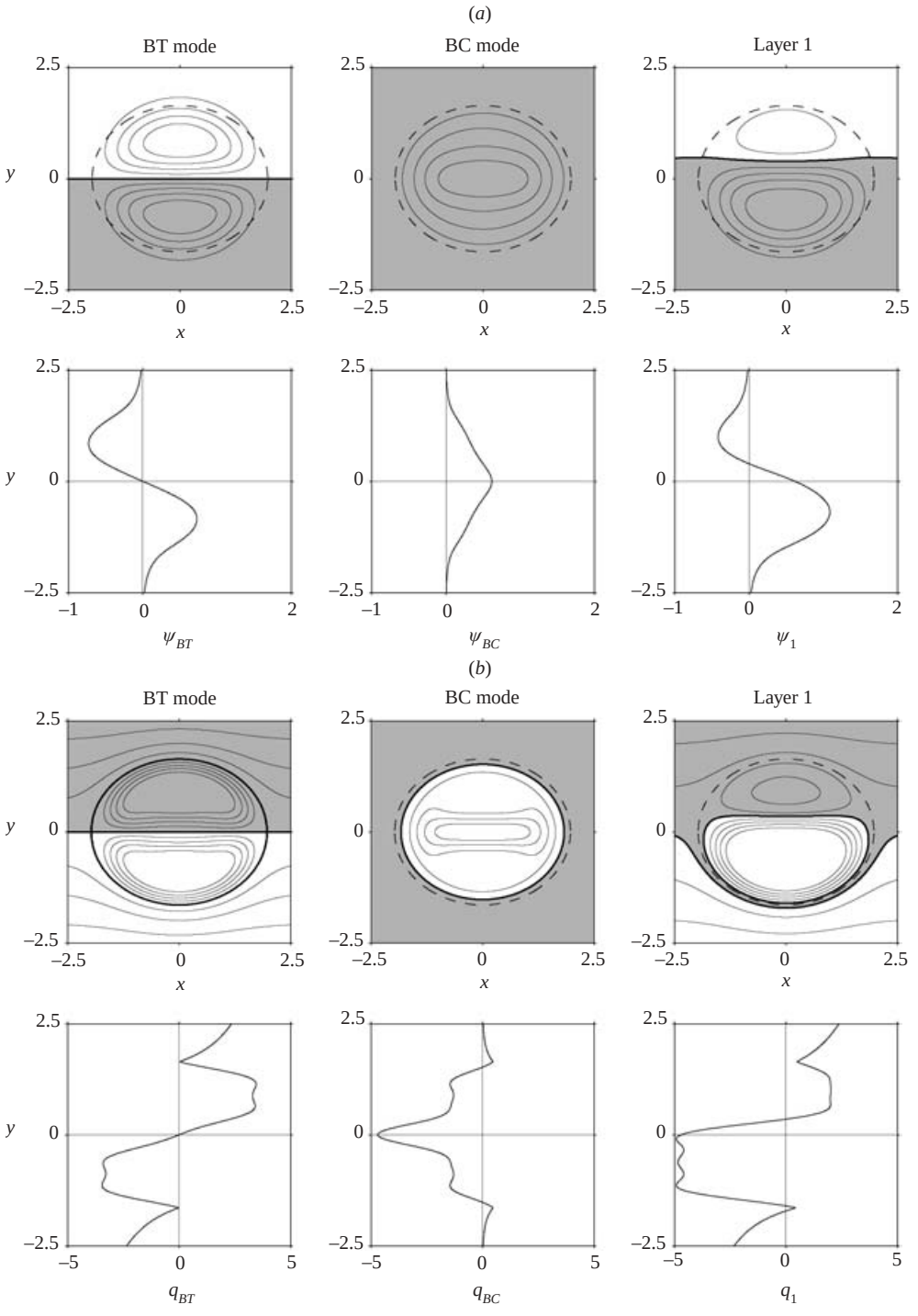

FIGURE 6. The extraordinary elliptical modon given by the parameters $U = 0.15$, $r_0 = 1.8$, $r_x/r_y = 1.2$ and labelled B in figure 4: (*a*) streamfunction fields (ψ); (*b*) PV fields. Notation as in figure 1.

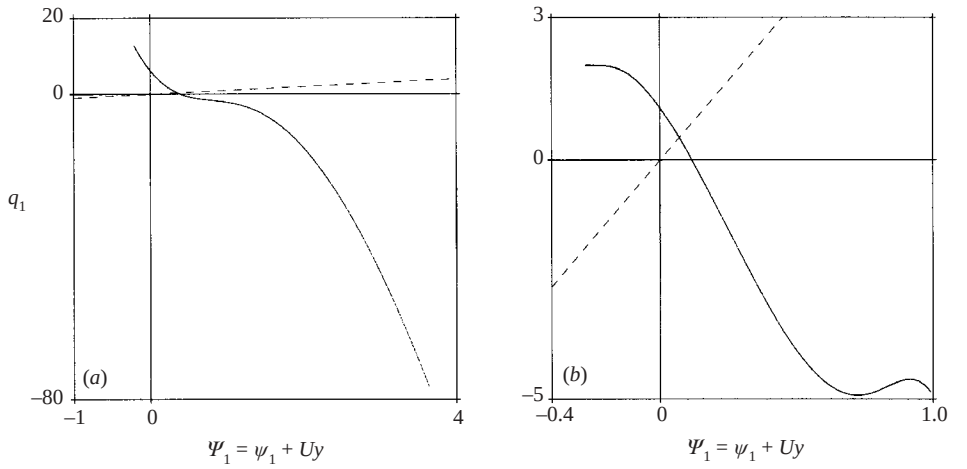

FIGURE 7. PV vs. Ψ scatter-graph for the upper layer: (*a*) ordinary elliptical modon shown in figure 5; (*b*) extraordinary elliptical modon shown in figure 6. Notation as in figure 3.

both streamfunction and PV. In particular, the layer PV field is a relatively small patch of one sign surrounded by a thick ring, in which the PV is smaller in absolute value and opposite in sign (figures 9*b* and 10*b*). A remarkable new property of a shielded elliptical modon is the ramification of the interior scatter-graph (figure 11). This is due to the fact that the interior domain in the first layer breaks down into two regions in which different dependences of q_1 vs. Ψ_1 hold. These regions are separated by a closed contour $\Gamma^{(In)}$ along which q_1 is constant (dotted lines in figures 9*b* and 10*b*). The contour $\Gamma^{(In)}$ bounds the central region and encloses an asymmetric dipole made up of the patch of strong vorticity and a weaker vortex of the opposite sign. The outer ring bounded by the contours Γ and $\Gamma^{(In)}$ contains two asymmetric 'banana-like' vortices and their peripheries (figures 9*b*, 10*b*). The longer branch on left side of the scatter-graph corresponds to the central region, and the shorter to the outer ring. Some asymmetry of the contour $\Gamma^{(In)}$ means that, in the second layer, the corresponding internal contour does not coincide with $\Gamma^{(In)}$, but is symmetric to $\Gamma^{(In)}$ about the x-axis.

A ramification of the interior scatter-graph is a general property of shielded non-circular (nonlinear) modons – those consisting of vortical pairs enclosed in vorticity rims. The absence of ramification is an inherent feature of circular shielded modons in which the two interior scatter-graphs coincide due to their linearity.

4.3. *Accuracy*

The accuracy of the computational algorithm described in § 3 is a function of its parameters N, P, K and the tolerance (or the number of iterations) specified for the successive linearization procedure, as well as of the form of the contour Γ and the intrinsic parameters U and C of the problem (9), (10), (24), (25). We tested the method for different combinations of parameters, in most cases Γ being an ellipse. The general conclusion is that the stronger the deviation from a circle, the lower the accuracy if all the other parameters are fixed. At a given Γ, the accuracy generally decreases with increasing C. Within the interval $0.1 \leqslant U \leqslant 1.5$ the accuracy is practically independent of U; outside this interval it decreases with decreasing or increasing U. On the other hand, at fixed Γ, U and C, the computational errors have a tendency to decrease when N, P and K are increased. We also note that a

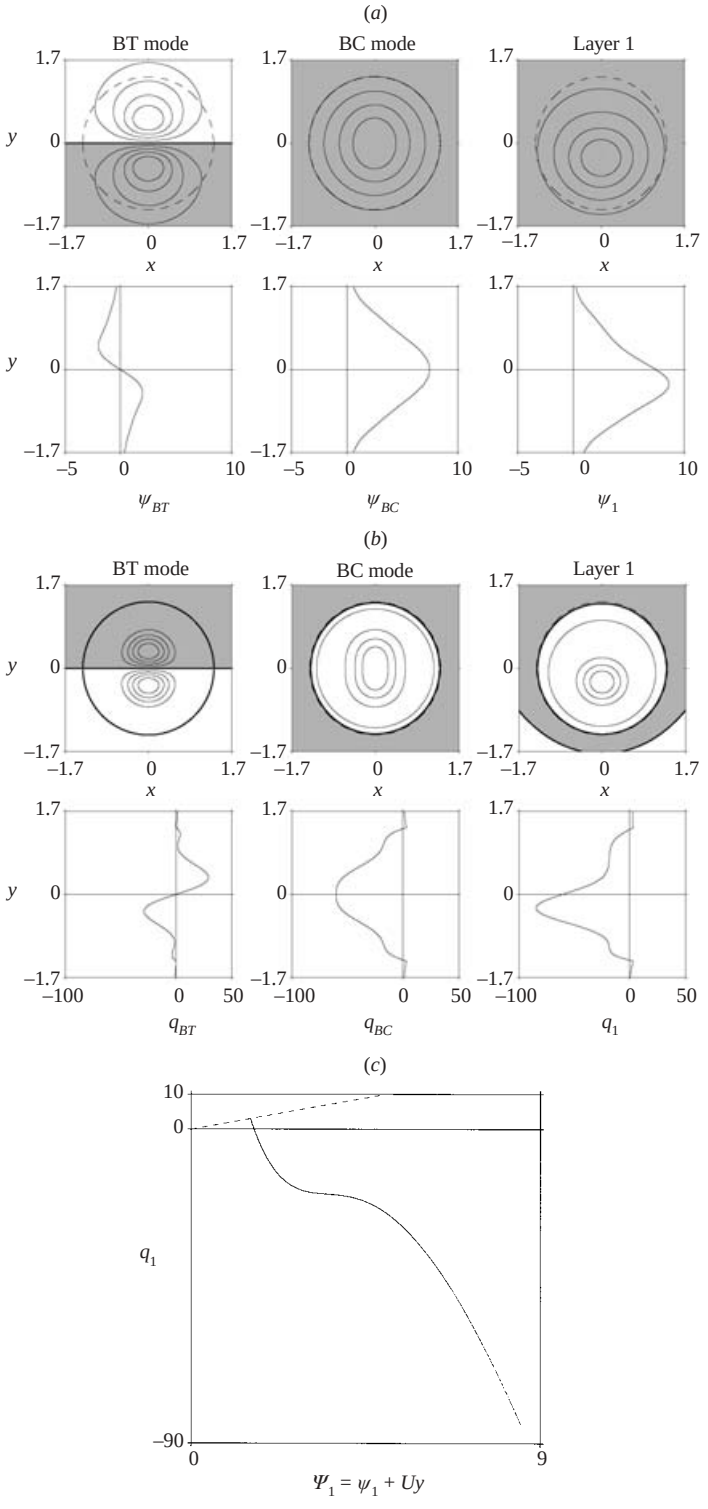

FIGURE 8. The ordinary elliptical modon given by the parameters $U = 0.5$, $r_0 = 1.35$, $r_y/r_x = 1.05$ and labelled C in figure 4: (*a*) streamfunction fields (ψ); (*b*) PV fields; (*c*) scatter-graph. Notation as in figures 1 and 3.

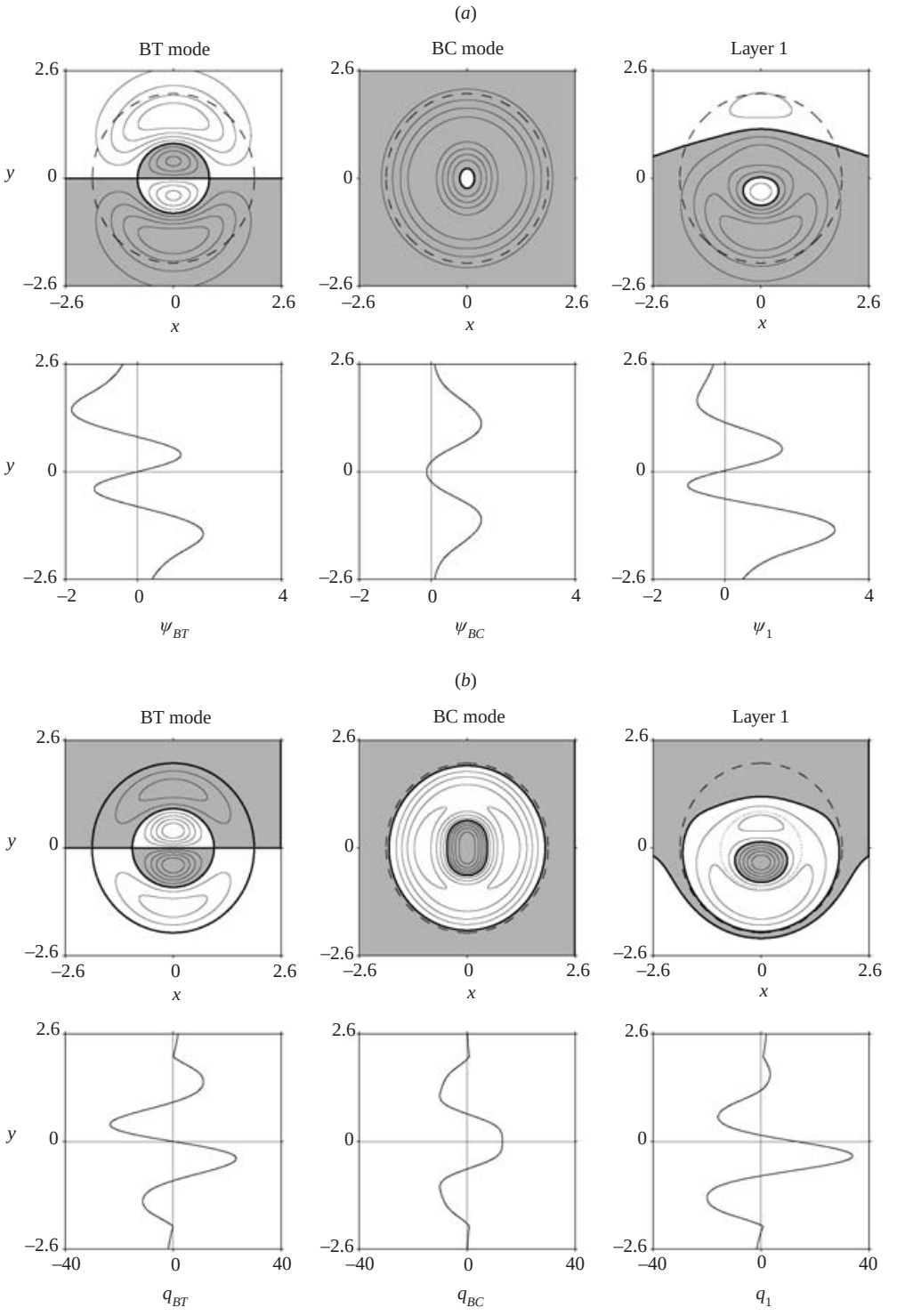

FIGURE 9. The shielded ordinary elliptical modon given by the parameters $U = 0.5$, $r_0 = 2$, $r_y/r_x = 1.05$ and labelled D in figure 4: (*a*) streamfunction fields (ψ); (*b*) PV fields. Dotted line, internal separatrix $\Gamma^{(In)}$; other notation as in figure 1.

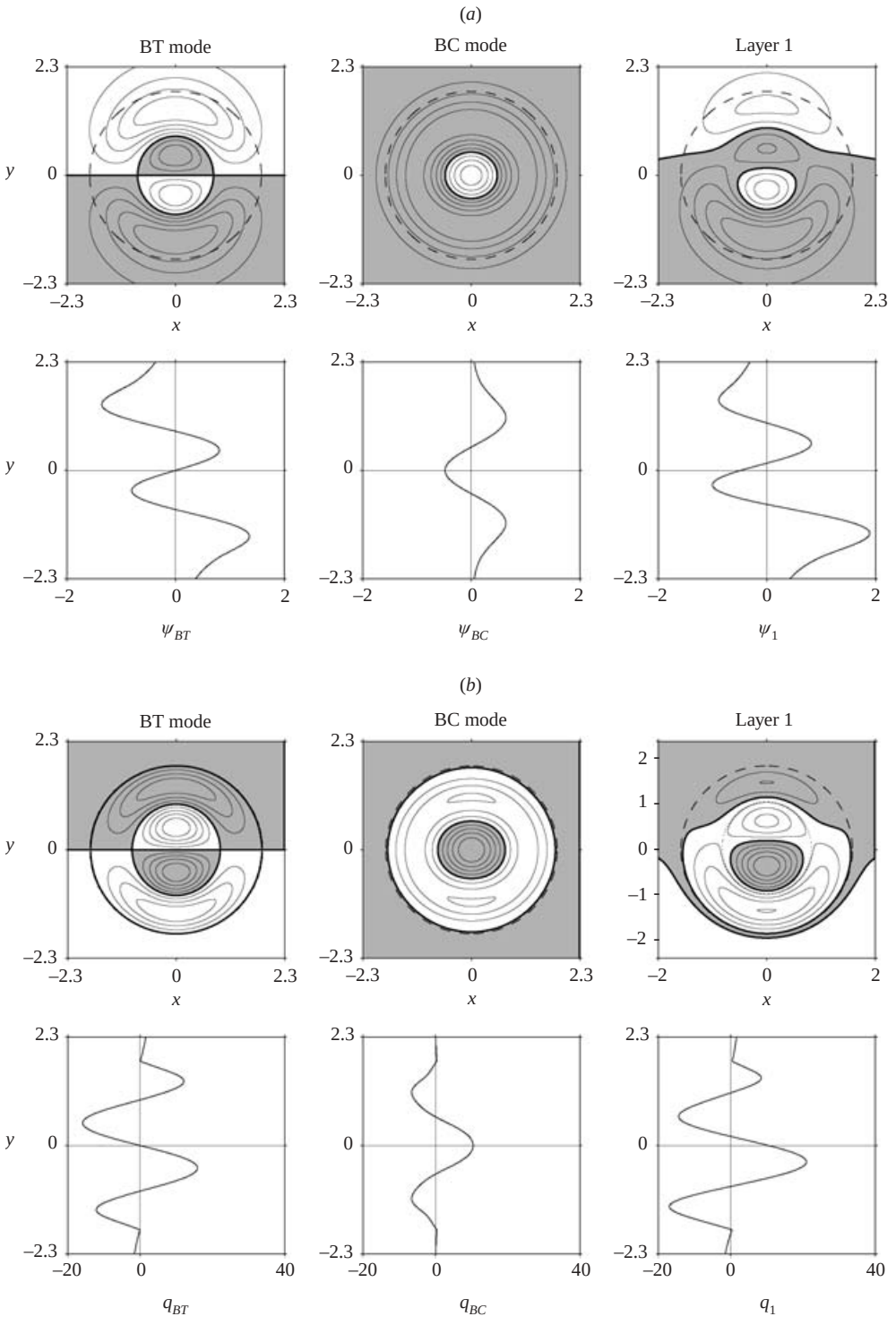

FIGURE 10. The shielded extraordinary elliptical modon given by the parameters $U = 0.5$, $r_0 = 1.8$, $r_x/r_y = 1.02$ and labelled E in figure 4: (*a*) streamfunction fields (ψ); (*b*) PV fields. Notation as in figures 1 and 9.

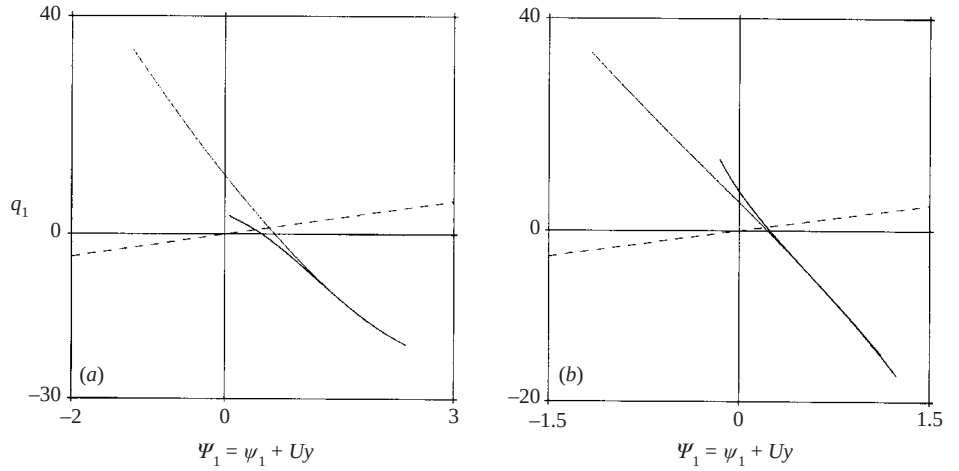

FIGURE 11. The upper-layer PV vs. Ψ scatters for shielded elliptical modons: (*a*) ordinary modon shown in figure 9; (*b*) extraordinary modon shown in figure 10. Notation as in figure 3.

N	mean Res eq. (32)	max Res eq. (32)	mean Res eq. (33)	max Res eq. (33)
7	0.029020	0.090037	0.027892	0.078470
9	0.004238	0.015539	0.004451	0.013487
11	0.000696	0.002576	0.001601	0.006920
13	0.000907	0.004186	0.001207	0.005017
15	0.000077	0.000404	0.000252	0.002609

TABLE 1. The root-mean-square and maximal residuals in equations (32) and (33) at the output of the iterative procedure.

N	mean Ψ_Γ	max Ψ_Γ	mean $\left[\frac{\partial\Psi}{\partial n}\right]_\Gamma$	max $\left[\frac{\partial\Psi}{\partial n}\right]_\Gamma$	mean q_Γ	max q_Γ
7	0.017887	0.023873	0.051210	0.084416	0.223252	0.296012
9	0.001203	0.002014	0.006400	0.012597	0.016973	0.029934
11	0.000948	0.001356	0.005226	0.009454	0.013362	0.018972
13	0.000292	0.000466	0.001657	0.003367	0.004322	0.007216
15	0.000066	0.000110	0.000406	0.000758	0.000977	0.001655

TABLE 2. The root-mean-square and maximal values of the interior barotropic variables at the separatrix.

certain correspondence between N, P and K (or h) must be established to avoid possible oscillations of the polynomials between the grid points on the one hand, and to minimize the necessary computations, on the other. The general rule is that higher-degree polynomials require smaller mesh size. Our tests show that if the ratio r_y/r_x or r_x/r_y does not exceed the limit of 1.2, quite a high accuracy can be achieved at $N = 11$, $P = 300$, $h = r_0/30$ (i.e. $K \approx 700$).

In tables 1–3, the dependence of the accuracy estimates upon the parameter N is shown for an extraordinary elliptical modon given by the parameters: $r_0 = 1.3$, $r_x/r_y = 1.1$, $U = 1$, $C = 0.1$, the maximal number of iterations allowed being fixed. The resulting maximal barotropic and baroclinic streamfunction and PV values

N	mean$[\Psi]_\Gamma$	max$[\Psi]_\Gamma$	mean$\left[\frac{\partial\Psi}{\partial n}\right]_\Gamma$	max$\left[\frac{\partial\Psi}{\partial n}\right]_\Gamma$	mean $\tilde{q}_\Gamma$	max $\tilde{q}_\Gamma$
7	0.002699	0.005989	0.007380	0.015512	0.030157	0.066729
9	0.000151	0.000276	0.000503	0.000803	0.002533	0.004667
11	0.000014	0.000020	0.000175	0.000405	0.000212	0.000421
13	0.000019	0.000044	0.000145	0.000384	0.000345	0.000770
15	0.000009	0.000013	0.000045	0.000076	0.000127	0.000195

TABLE 3. The root-mean-square and maximal values of the interior baroclinic variables at the separatrix.

(needed to judge the relative errors) are: max $\Psi_{BT} \approx 2$, max $\Psi_{BC} \approx 0.6$, max $q_{BT} \approx 10$, max $q_{BC} \approx 6$. At the stage of constructing the first-approximation solution, unequal mesh sizes were specified for the x- and y-axes: $h_x = r_x/30$, $h_y = r_y/30$; the number of boundary points being taken to be $P = 300$. For checking the accuracy at which equations (32) and (33) were satisfied, a fine 200×200 mesh was used (i.e. $h_x = r_x/200$, $h_y = r_y/200$, about 31 400 points), and the fulfillment of the boundary conditions and the constancy of the interior baroclinic PV along the separatrix were checked at 1000 points; only the first quadrant was considered. In the headings of tables 1–3 the following notations are used: mean Res – root-mean-square residual, i.e. the mean (over about 31 400 fine-mesh points) of the right-hand side of equation (32) or (33) at the output of the iterative procedure (30), (31); max Res – the corresponding maximal absolute residual; mean Ψ_Γ and max Ψ_Γ – the root-mean-square (over 1000 boundary points) and the maximal value, respectively, of Ψ_{BT} at the separatrix; mean q_Γ and max q_Γ – the same for q_{BT}; mean$[\Psi]_\Gamma$ and max$[\Psi]_\Gamma$ – the same for the jump of the baroclinic streamfunction (i.e. $|\Psi_{BC} - \Psi_{BC}^{(Ex)}|_\Gamma$); mean$[\partial\Psi/\partial n]_\Gamma$ and max$[\partial\Psi/\partial n]_\Gamma$ – the same for the jump of the normal-to-Γ derivative of the barotropic (table 2) and baroclinic (table 3) PV; mean $\tilde{q}_\Gamma$ and max $\tilde{q}_\Gamma$ – the same for the deviation of the interior baroclinic PV, q_{BC}, from its arithmetic mean.

The data presented in tables 1–3 prove that the errors decrease considerably when parameter N increases from 7 to 11, and less rapidly when N is increased from 11 to 15 (the latter is probably due to the limited precision provided by the software used). The accuracy achieved at $N = 11$ is indeed sufficient, as confirmed by the extreme thinness of the scatter-graphs in figures 3, 7, 8*c*, 11. We note that for a circular modon ($U = 0.5$, $r_0 = 1.3$, $C = 0.1$) the procedure converged very rapidly, giving at $N = 11$ errors within the interval 10^{-14} to 2×10^{-12}, the maximal values of the streamfunctions and PV being max $\Psi_{BT} \approx 2$, max $\Psi_{BC} \approx 0.5$, max $q_{BT} \approx 15$, max $q_{BC} \approx 4$.

5. Smoothness and stability

Our earlier numerical experiments (KBK) show that smooth circular baroclinic modons are quite durable, propagating steadily until $t = 200$ to 250 if the amplitude ratio $A_{BC}/A_{BT} = \max|\Psi_{BC}|/\max|\Psi_{BT}|$ is in the range approximately from 1 to 1.5 (here t is non-dimensional time, the scale being $T = 1/\beta L_{Ro}$). With a stronger baroclinic rider, the modon sheds a westward-travelling heton-like vortical pair and transforms into a smaller, nearly circular modon, whose radius and translation speed fit the dispersion relation $r_0 = r_C(U)$ for smooth circular modons (for details see KBK). Weak (but non-zero) riders induce gradual disintegration of the vortex structure,

which can be interpreted as indication of instability of barotropic Larichev–Reznik modons to baroclinic perturbations.

To clarify the stability properties of the smooth and non-smooth modons (i.e. those marked by continuity or discontinuity of the baroclinic PV), we conducted a number of experiments using the same simulation model. It is based on the non-dimensional equations of PV conservation for a two-layer ideal fluid (i.e. in a strictly inviscid limit) that are integrated in a rectangular domain $[-X < x < X; -Y < y < Y]$ with periodic conditions at $x = \pm X$ and conventional conditions

$$\frac{\partial \psi^{(j)}}{\partial x} = 0 \text{ and } \int_{-X}^{X} \frac{\partial^2 \psi^{(j)}}{\partial t \partial y} \, dx = 0 \quad \text{at} \quad y = \pm Y$$

(e.g. Kamenkovich *et al.* 1986, Ch. 2). The domain half-sizes X and Y were taken equal to $15L_{Ro}$, i.e. approximately 10 to 15 times larger than the modon radius, the space resolution being 15 and 30 nodes per mean modon radius for smooth and non-smooth modons, respectively; the time step was controlled by the gradients of Ψ and q and did not exceed $2.5 \times 10^{-3}T$.

In the experiments with non-smooth modons, the model was initialized using circular modons with separatrix radius both smaller and larger than the radius $r_C(U)$ of a smooth circular modon propagating at the speed U, the amplitude ratio A_{BC}/A_{BT} being equal to unity. Apart from their sizes, the circular modons with $r_0 < r_C(U)$ and $r_0 > r_C(U)$ at $A_{BC}/A_{BT} = 1$ differ in the character of the cross-sections of the layer relative vorticity in the y-direction (at $x = 0$): in the smaller modons the relative vorticity is monotonic when followed from the pole (point of extremum) outwards via the point of jump, while in the larger modons it is not. In two such modons, whose evolution is shown in figure 12, the initial parameters are: $A_{BC}/A_{BT} = 1, U = 0.5, r_0 = 0.5r_{0.5}$ (figure 12*a*) and $A_{BC}/A_{BT} = 1, U = 0.5, r_0 = 1.5r_{0.5}$ (figure 12*b*), where $r_{0.5} = r_C(0.5) \approx 1.30$ is the radius of a smooth circular modon that propagates at translation speed 0.5. These solutions differ also in that, in the smaller modon, the internal and external values of q_1 along the separatrix are of the same sign, whereas in the larger modon they are opposite in sign (cf. upper panels in figure 12*a*, *b*).

In contrast to the robustness of the smooth circular modon given by the above values of A_{BC}/A_{BT} and U, the evolution of the non-smooth vortices attests to their instability. The upper and lower vortices constituting the smaller modon ($r_0 = 0.5r_{0.5}$) start separating almost immediately. Their drift is similar to some extent to that of two non-interacting barotropic monopoles (the effect of the weak accompanying vortices is negligible). While radiating Rossby waves and emitting vorticity filaments, one of them (depending on the sense of rotation) translates mainly westwards with a relatively small southward component of propagation; the other vortex translates symmetrically about the x-axis (figure 12*a*). There is also some degree of similarity in this evolution to that of a dipole with a weak smooth baroclinic rider (cf. KBK).

The evolution of small non-smooth circular modons that are sufficiently close in size to the smooth ones differs from the scenario described above. For example, a modon, whose nominal translation speed and radius are 0.5 and $0.9r_{0.5}$, respectively, by $t \approx 15$ reorganizes into a slightly oval (and weakly nonlinear) essentially smooth structure of nearly the same radius and, subsequently propagates steadily at a speed $U \approx 0.55$.

The larger vortex ($r_0 = 1.5r_{0.5}$) evolves in a manner similar to that of a smooth modon with a strong rider: the peripheral westward parts of the vortices in the upper

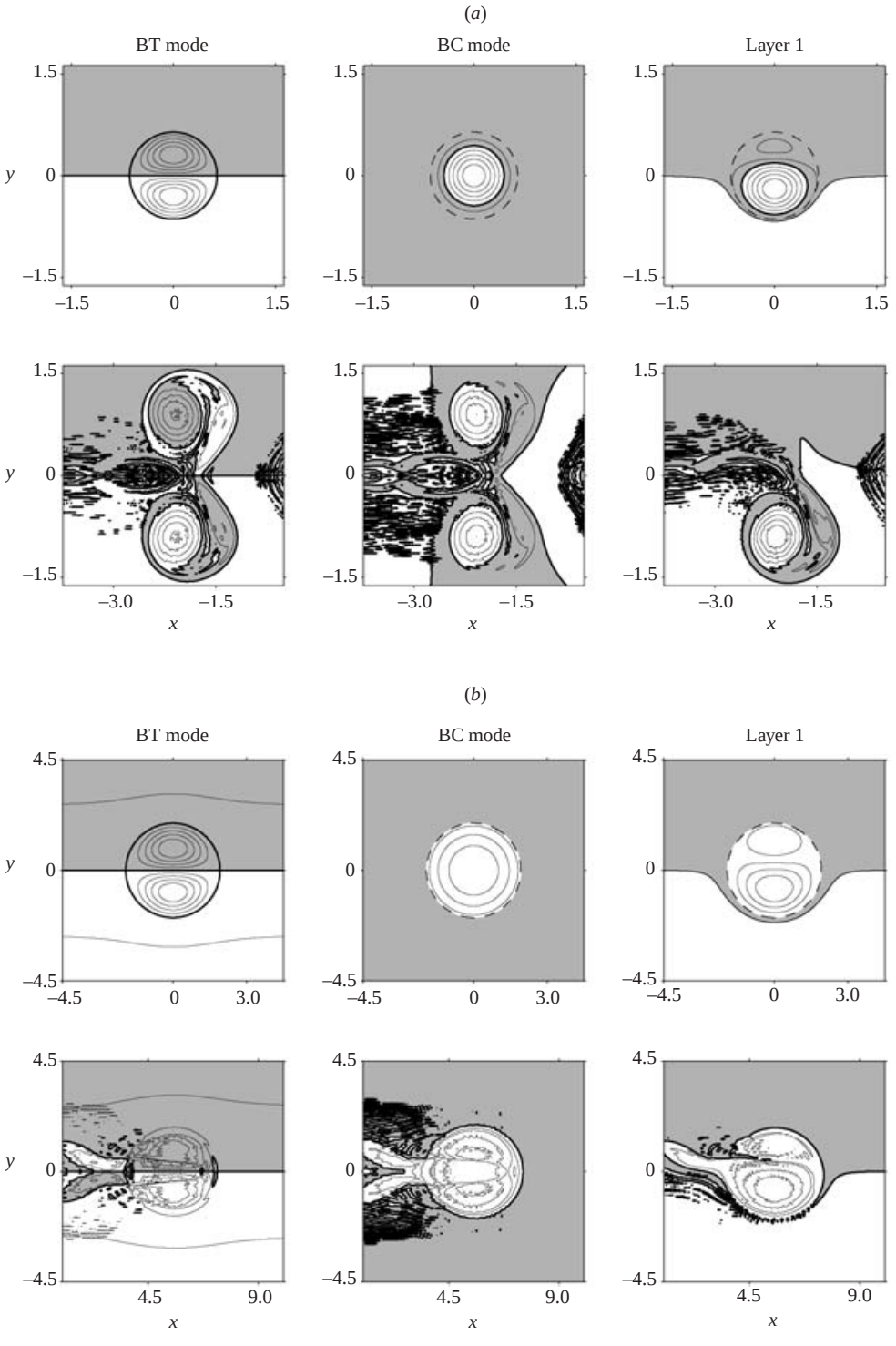

FIGURE 12. Evolution of the PV fields of two initially non-smooth circular modons given by the parameters: $U = 0.5$, $A_{BC}/A_{BT} = 1$; and (*a*) $r_0 = 0.5r_{0.5} \approx 0.65$, (*b*) $r_0 = 1.5r_{0.5} \approx 1.95$. Upper panel, initial state ($t = 0$); lower panel, the fields at $t = 5$. Notation as in figure 1.

and the lower layers elongate and overlap, which leads to shedding of a considerable amount of PV (figure 12*b*). After the separation, the remaining eastward vortex structure reorganizes into a circular modon composed of a dipolar barotropic mode and a smooth baroclinic rider. This process was detailed in our previous publication (KBK). Smaller circular modons, whose radii still exceed that of a smooth circular modon, evolve in much the same way.

The unstable dynamics of the two types of non-smooth modons (with $r_0 < r_C(U)$ and $r_0 > r_C(U)$) should not be associated with the problem of resolving a PV jump in a finite-difference model. Indeed, numerical experiments with the Stern modon using a barotropic version of this numerical model (Kizner & Berson 2000) prove that even at mesh size twice as large, when about 15 mesh points fall within the modon radius, the resolution is still good and the jump front can be observed in the PV field for quite a long time, at least till $t = 30$ (which is much longer than the characteristic time of the above unstable changes). Experiments with non-smooth baroclinic modons conducted at this halved resolution support the conclusion that their instability has a physical rather than a numerical origin: the simulated dynamics were exactly the same as at a high resolution.

The instability of the non-smooth barotropic modon-plus-rider solution was first demonstrated numerically by Swenson (1987). Although so far no strict analytical proof of this instability has been provided, it is conventionally attributed to the specificity of the radial velocity profile rather than to the PV jump (Swenson 1987; Nycander 2001). For Euler equations in two dimensions, Filippov & Yan'kov (1986) showed that stability of monopoles is guaranteed by the monotonic decrease of the radial profile of vorticity. It is possible that the shape of the layer relative vorticity profile is important in determining the stability or otherwise of two-layer modons on the β-plane as well. However, we have not found such qualitative distinctions between the vorticity profiles of circular smooth and smaller non-smooth modons (besides the vorticity continuity/discontinuity) that might clearly point to the stability of the first and instability of the latter. This suggests that the monotonic decrease of the relative vorticity profile does not represent a sufficient condition for the stability of baroclinic β-plane modons.

In smooth elliptical modons, due to the nonlinearity of the interior PV vs. streamfunction relation, the amplitude of the baroclinic mode is not arbitrary. This, however, does not imply that any smooth elliptical modon is necessarily stable. A few sample evolutionary tests (up to $t = 100$) suggest that smooth extraordinary modons are unstable. Regarding the ordinary modons, the closer the modon's size is to that of a smooth circular modon of the same translation speed, the more steady its propagation.

Smooth ordinary elliptical modons categorized by the inequality $r_0 < r_C(U)$ are generally rather robust if they are not too small. For example, the modon given by the parameters $U = 1, r_0 = 1, r_y/r_x = 1.1$ (figure 5) is relatively remote from the line of smooth circular modons $r_0 = r_C(U)$ (point A in figure 4). Yet, in an evolutionary simulation, it changes very little, a small change being visible only in the barotropic PV at the initial stage of the evolution.

In a bigger smooth ordinary modon given by the parameters $U = 0.4$, $r_0 = 1.14$, $r_y/r_x = 1.07$ (point F in figure 4), which is closer to the line $r_0 = r_C(U)$, no evolutionary trends are evident at least up to $t = 350$ (figure 13*a*). In contrast, the smooth extraordinary modon whose initial parameters are $U = 0.4, r_0 = 1.45, r_x/r_y = 1.07$ (point G in figure 4) evolves considerably within a few tens of T (figure 13*b*). The growing changes in the modon structure and translation speed result in its

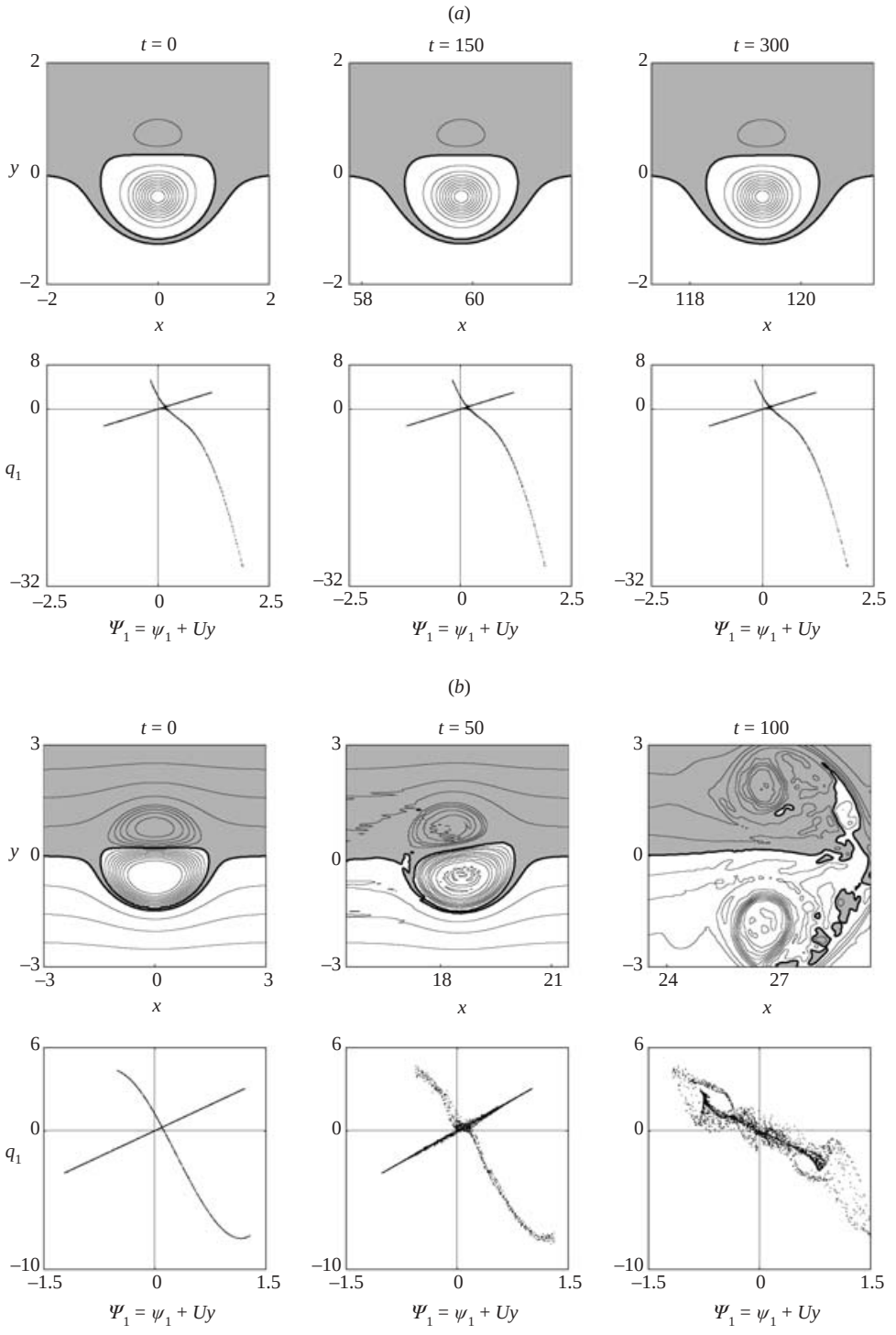

FIGURE 13. Evolution of two smooth elliptical modons given by the parameters: $U = 0.4$, $r_y/r_x = 1.07$; and (*a*) $r_0 = 1.14$, (*b*) $r_0 = 1.45$ (labelled F and G respectively in figure 4). Upper panel, contours of constant PV (the interval is 10% of the maximum; regions of positive values are shadowed); lower panel, PV vs. Ψ scatter-graphs.

disintegration by $t = 90$, the translation speed being estimated from the change of the x-coordinate of the barotropic PV poles in time.

The smooth ordinary elliptical modon given by the parameters $U = 0.5$, $r_0 = 1.35$, $r_y/r_x = 1.02$ (figure 8) and belonging to the region $r_0 > r_C(U)$ (point C in figure 4) displays less stable behaviour. By $t = 15$ it has converted into a steadily translating (at $U \approx 2.5$) non-circular modon of approximately the same mean radius. We believe that this evolution is related primarily to the strength of the baroclinic mode in the solution ($A_{BC}/A_{BT} \approx 3.8$). In such a vortical pair, the shift between the poles of the upper and lower vortices is insufficient to permit an efficient hetonic interaction between the vortices. Thus the modon increases its ellipticity, strengthens the barotropic mode and speeds up. Efforts to construct a smooth ordinary elliptical solution at $U = 2.5$ have not been successful for reasons of divergence of the successive linearization procedure.

In evolutionary experiments, shielded elliptical modons displayed strongly unstable behaviour, which might be anticipated based on the strong instability of the circular shielded barotropic modons (Kizner & Berson 2000).

6. Conclusion

Circular modons represent only a sub-class of possible modon solutions. Despite the fact that the equivalence of the linearity of the PV vs. Ψ dependence within the trapped-fluid domain and the circularity of the latter was not understood immediately, the possibility, in many cases, of constructing analytical solutions has stimulated the interest of researchers in the circular modons (Stern 1975; Larichev & Reznik 1976; Flierl *et al.* 1980; Berestov 1979; Kizner 1984, 1997; Reznik & Sutyrin 2001). However, one could hardly expect that real robust vortical structures in stratified geophysical fluids would necessarily exhibit circularity and linearity (in the above sense).

Numerical simulations (KBK) indicate that although circular modons with moderately strong baroclinic riders are quite robust, some types of perturbations may induce transitions of these modons to even more stable oval states (in an equal-depth two-layer model); transitions of this kind were also observed in a three-layer model. We believe that such non-circular heton-like vortical structures may represent a fairly general type of baroclinic equilibrium in geophysical fluids.

In order to facilitate the analysis of non-circular modons, a mathematical problem was considered for the solutions categorized by the symmetry of their interior areas about the x- and y-axes. A numerical method for constructing such modons was suggested based on the successive linearization of the governing equations and polynomial approximation of the corrections. We cannot deduce the correctness of the above nonlinear problem exactly (in analytical terms), but it is supported by the fact that, whenever the numerical procedure converges, the resulting solution is unique. In particular, specifying a non-circular separatrix always results in the nonlinearity of the interior PV vs. Ψ dependence in the layers, whereas circular modons are always linear.

As well as the non-smooth solutions, in which a finite jump of the baroclinic PV along the separatrix is permissible, smooth modons were also shown to exist. Smooth solutions (those with no jump in the baroclinic PV at the separatrix) are available when a dispersion relationship between the modon size, shape, translation speed and the exterior baroclinic amplitude is fulfilled. Numerical simulations conducted indicate that non-smooth solutions are presumably unstable, whereas among smooth modons some display substantial durability.

In our efforts to obtain modons similar in their properties to those that emerged in the simulations of KBK, we focused upon elliptical figures and found that the branches of the dispersion relation for the smooth circular modons, $r_0 = r_C(U)$, break the (r_0, U)-plane down into regions where different types of elliptical modons exist. Beneath the lower branch of this relation, at $r_0 < r_C(U)$, only non-shielded elliptical solutions were found characterized by the inequality $r_y > r_x$ (ordinary modons). In contrast, non-shielded solutions, in which $r_y < r_x$ (extraordinary modons), were found only above this line. On and above it – at $r_0 \geqslant r_C(U)$ – ordinary modons are also present, but they differ in structure from the ordinary modons occurring beneath this line.

In regard to the baroclinic mode, the ordinary elliptical solutions at $r_0 < r_C(U)$ are similar to the quasi-stable oval modons obtained in the evolutionary simulations of KBK: the baroclinic PV field in the ordinary modons normally has a saddle-like shape. The ordinary modons of the first type ($r_0 < r_C(U)$) typically demonstrate a considerable durability if they are not too distant from the line $r_0 = r_C(U)$. They can hardly be regarded as direct analogues of the oval modons described by KBK, however, since the latter fall within the region $r_0 > r_C(U)$. On the other hand, our experiment with the ordinary elliptical modon of the second type ($r_0 > r_C(U)$) proves its instability.

These observations, along with the fact that even small perturbations of the separatrix form may lead to considerable changes in the structure of the resulting modon solution, lead us to believe that the oval modons obtained in the evolutionary experiments are not exactly elliptical. Moreover, one should not rule out the possibility that they have two different (though symmetrical and almost indistinguishable) separatrices in the upper and lower layers. We believe that extended numerical research should be carried out to evaluate the dispersion relation $r_0 = r_0(U, C, r_y/r_x)$ for the smooth elliptical modons as a three-dimensional surface in the four-dimensional space of the parameters U, C, $r_y/r_x, r_0$. Implementation of such a program would require a considerable effort, but determining the topology and geometry of the dispersion surface may turn out to be crucial in understanding the causes of the stability of some modons and instability of others. Another issue that is likely to be clarified in the framework of such research is why, in the super long-term evolutionary simulations (KBK), the substantially robust circular modons eventually leap to more or less remote oval states instead of passing close to neutrally stable oval states, that is, 'creeping' along the dispersion surface.

One more possible application of our numerical procedure in its present form is a detailed study of non-circular barotropic modons. Whereas in smooth baroclinic modons the bulk computations are related to finding the proper value of the constant C, in barotropic modons $C = 0$, and only one equation, $J(\Psi_{BT}, q_{BT}) = 0$, supplemented with one pair of boundary conditions (the first ones in (24) and (25)) must be solved. This makes possible a comparative study of the properties of barotropic modons of different types, including propagating and standing (and thus non-smooth) modons on both the β- and f-planes. A comparison of the behaviour of barotropic and baroclinic modons in evolutionary simulations is also of great interest because such a study might reveal the role of baroclinicity in the transition of linear (circular) modons to nonlinear oval states.

The methodological ideas underlying the approach presented in § 3 open up the prospect of conducting a study of non-symmetrical modons. Asymmetry, in general (whether or not the layers are of the same depths), means the lack of antisymmetry and symmetry in the barotropic and baroclinic modes, respectively, and allows the existence of two different separatrices, Γ_1 and Γ_2, in the upper and lower layers.

Accordingly, it yields the presence of two free constants, $\Psi_1|_{\Gamma_1} = C_1$ and $\Psi_2|_{\Gamma_2} = C_2$, in a modon solution, once the translation speed is fixed.

This research was supported by The Israel Science Foundation (grant # 616/00). We are grateful to the anonymous referees for helpful comments on the manuscript. We also thank G. Reznik and E. Benilov for stimulating discussions.

REFERENCES

Berestov, A. L. 1979 Solitary Rossby waves. *Izv. Akad. Sci., USSR, Atmos. Oceanic Phys.* **15**, 648–651.

Boyd, J. P. 2001 *Chebyshev and Fourier Spectral Methods*, 2nd edn. Dover.

Boyd, J. P. 2002 A comparison of numerical algorithms for Fourier extension of the first, second, and third kinds. *J. Comput. Phys.* **178**, 119–160.

Boyd, J. P. & Ma, H. 1990 Numerical study of elliptical modons using spectral methods. *J. Fluid Mech.* **221**, 597–611.

Chaplygin, S. A. 1903 One case of vortex motion in fluid. *Trans. Phys. Sect. Imperial Moscow Soc. Friends of Natural Sciences* **11**, N 2, 11–14 (in Russian).

Filippov, D. V. & Yan'kov, V. V. 1986 Two-dimensional electron vortices. *Sov. J. Plasma Phys.* **12**, 548–552.

Flierl, G. R., Larichev, V. D., McWilliams, J. C. & Reznik, G. M. 1980 The dynamics of baroclinic and barotropic solitary eddies. *Dyn. Atmos. Oceans* **5**, 1–41.

Flierl, G. R., Stern, M. E. & Whitehead Jr, J. A. 1983 The physical significance of modons: Laboratory experiments and general integral constraints. *Dyn. Atmos. Oceans* **7**, 233–264.

van Geffen, J. H. G. M. & van Heijst, G. J. F. 1998 Viscous evolution of 2D dipolar vortices. *Fluid Dyn. Res.* **22**, 191–213.

Gryanik, V. M. 1983 Dynamics of singular geostrophic vortices in a two-layer model of the atmosphere (or ocean). *Bull. (Izv.) Acad. Sci. USSR, Atmos. Oceanic Phys.* **19**, 171–179.

Gryanik, V. M. 1988 Localized vortical disturbances, "vortex charges" and "vortex filaments" in a Baroclinic, differentially rotating fluid. *Bull. (Izv.) Acad. Sci. USSR Atmos. Oceanic Phys.* **24**, 919–926.

Hesthaven, J. S., Lynov, J. P., Nielsen, A. H., Rassmussen, J. J., Schmidt, M. R., Shapiro, E. G. & Turitsyn, S. K. 1995 Dynamics of a nonlinear dipole vortex. *Phys. Fluids* **7**, 2220–2229.

Hogg, N. G. & Stommel, H. M. 1985 The heton, an elementary interaction between discrete baroclinic geostrophic vortices, and its implications concerning eddy heat-flow. *Proc. R. Soc. Lond.* A **397**, 1–20.

Kamenkovich, V. M., Koshlyakov, M. N. & Monin, A. S. 1986 *Synoptic Eddies in the Ocean.* Reidel.

Kantorovich, L. V. 1948 Functional analysis and applied mathematics. *Yspekhi Matem. Nauk* **3**, 89–185 (in Russian).

Kizner, Z. I. 1984 Rossby solitons with axisymmetric baroclinic modes. *Dokl. USSR Acad. Sci.* **275**, 1495–1498.

Kizner, Z. I. 1988 On the theory of intrathermocline eddies. *Dokl. USSR Acad. Sci.* **300**, 453–457.

Kizner, Z. I. 1997 Solitary Rossby waves with baroclinic modes. *J. Mar. Res.* **55**, 671–685.

Kizner, Z. & Berson, D. 2000 Emergence of modons from collapsing vortex structures on β-plane. *J. Mar. Res.* **58**, 375–403.

Kizner, Z., Berson, D. & Khvoles, R. 2002 Baroclinic modon equilibria on the beta-plane: Stability and transitions. *J Fluid Mech.* **468**, 239–270 (referred to herein as KBK).

Koshliakov, N. S., Gliner, E. B. & Smirnov M. M. 1962 *Differential Equations of Mathematical Physics.* Nauka, Moscow.

Lamb, H. 1895 *Hydrodynamics*, 2nd edn. Cambridge University Press.

Lamb, H. 1906 *Hydrodynamics*, 3rd edn. Cambridge University Press.

Larichev, V. D. & Reznik, G. M. 1976 Two-dimensional solitary Rossby waves. *Rep. USSR Acad. Sci.* **231**, 1077–1080.

Meleshko, V. V. & van Heijst, G. J. F. 1994 On Chaplygin's investigations of two-dimensional vortex structures in an inviscid fluid. *J. Fluid Mech.* **272**, 157–182.

McWilliams, J. C., Flierl, G. R., Larichev, V. D. & Reznik, G. M. 1981 Numerical studies of barotropic modons. *Dyn. Atmos. Oceans* **5**, 219–238.

McWilliams, J. C. & Zabusky, N. J. 1982 Interactions of isolated vortices. I: Modons colliding with modons. *Geophys. Astrophys. Fluid Dyn.* **19**, 207–227.

Morel, Y. & McWilliams, J. 1997 Evolution of isolated interior vortices in the ocean. *J. Phys. Oceanogr.* **27**, 727–748.

Nielsen, A. H. & Juul Rasmussen, J. 1997 Formation and temporal evolution of the Lamb-dipole. *Phys. Fluids* **9**, 982–991.

Nycander, J. 1988 New stationary vortex solutions of the Hasegawa-Mima equation. *J. Plasma Phys.* **39**, 418–428.

Nycander, J. 2001 Drift velocity of rotating quasigeostrophic vortices. *J. Phys. Oceanogr.* **31**, 2178–2185.

Reznik, G. M. & Sutyrin, G. G. 2001 Baroclinic topographic modons. *J. Fluid. Mech.* **437**, 121–142.

Stern, M. E. 1975 Minimal properties of planetary eddies. *J. Mar. Res.* **33**, 1–13.

Sutyrin, G. G., Hesthaven, J. S., Lynov, J. P. & Juul Rasmussen, J. 1994 Dynamical properties of vortical structures on the beta-plane. *J. Fluid Mech.* **268**, 103–131.

Swenson, M. 1987 Instability of equivalent-barotropic riders. *J. Phys. Oceanogr.* **17**, 492–506.

Verkley, W. T. M. 1993 A numerical method to find form-preserving free solutions of the barotropic vorticity equation on a sphere. *J. Atmos. Sci.* **50**, 1488–1503.